

NON-LINEAR LEAST-SQUARES OPTIMIZATION OF RATIONAL FILTERS FOR THE SOLUTION OF INTERIOR EIGENVALUE PROBLEMS

JAN WINKELMANN* AND EDOARDO DI NAPOLI†

Abstract. Rational filter functions can be used to improve convergence of contour-based eigensolvers, a popular family of algorithms for the solution of the interior eigenvalue problem. We present a framework for the optimization of rational filters based on a non-convex weighted Least-Squares scheme. When used in combination with the FEAST library, our filters out-perform existing ones on a large and representative set of benchmark problems. This work provides a detailed description of : (1) a set up of the optimization process that exploits symmetries of the filter function for Hermitian eigenproblems, (2) a formulation of the gradient descent and Levenberg-Marquardt algorithms that exploits the symmetries, (3) a method to select the starting position for the optimization algorithms that reliably produces effective filters, (4) a constrained optimization scheme that produces filter functions with specific properties that may be beneficial to the performance of the eigensolver that employs them.

Key words. Hermitian eigenvalue problem, rational filters, contour integral, FEAST, subspace iteration

AMS subject classifications.

15A18, 65F10, 65F15, 65F50, 90C26

1. Introduction. The last ten years have witnessed a proliferation of papers on methods for the solution of the interior eigenvalue problem based on the use of the resolvent operator [10,22,24,25]. In practice, the spectrum of the eigenproblem can be “sliced” into multiple subspaces leading to the solution of quasi-independent sub-problems. Hence, these methods are considered to be part of the larger class of spectrum-slicing eigensolvers. In many instances a resolvent can be looked at as a rational function of the matrices defining the eigenvalue problem. In this paper we conduct a detailed investigation of how a carefully crafted rational function can improve the efficacy of resolvent-based eigensolvers. To this end, we initially adopt the conventional way to look at the resolvent as an approximation of an ideal filter represented by the standard indicator function. Then, the problem of finding a “good” rational function can be cast as one of 1) finding a continuous filter that approximates the discontinuous indicator function and, 2) improves the effectiveness of the eigensolver by providing an extensive analysis of the choice of parameters involved in the optimization process. We do not aim at a filter that is just an optimal approximation of the indicator function, but rather at a filter that is specifically crafted for the class of eigensolver we are interested in. Our method is based on a non-linear Least-Squares optimization approach, which leads to a series of custom filters we termed **S**ymmetric non-**L**inear **O**ptimized **L**east-**S**quares (SLiSe), read “slice”. Our work is a step towards problem-specific filters that are flexible enough to be capable of exploiting cheaply available information on the spectral structure of a given problem. Such an approach can result in an eigensolver with better performance and less parallel work-load imbalance. In addition, we provide an efficient procedure that allows for the generation of such filters at runtime.

The paper contains five major contributions:

Rich optimization framework. We illustrate an optimization framework, via weighted Least-Squares, based on the L_2 function norm instead of optimizing the rational function only at a number of sample points via the ℓ_2 norm (see [2]). The defined residual level function, its gradients, and an approximated Hessian are all based on the L_2 inner product. Such a setup allows for the use of the Levenberg-Marquardt method to solve for the non-linear Least-Squares problem. Flexibility is the landmark of the developed framework: we present penalty parameters and box constraints to obtain filters that, for example, are better suited for Krylov-based linear system solvers.

Symmetries of the resolvent for Hermitian matrices. We expose the intrinsic symmetries of the rational function approximating the indicator function. Such symmetries are then exploited in the implementation of the optimization process: filters which are invariant under conjugation

*Address: Aachen Institute for Advanced Study in Computational Engineering Science, RWTH Aachen University, Schinkelstr. 2, 52062-Aachen, Germany, winkelmann@aices.rwth-aachen.de

†Address: Jülich Supercomputing Centre, Institute for Advanced Simulation, Forschungszentrum Jülich GmbH, Wilhelm-Johnen strasse, 52425-Jülich, Germany. e.di.napoli@fz-juelich.de.

and parity transformations require fewer degrees of freedom, which results in faster numerical executions.

Optimization of pole placement. Optimizing the rational function’s poles and coefficients requires the solution of a non-convex problem. On the up side, this is a problem with a much richer parameter space enabling more sophisticated solutions. On the other hand, this is a much more complicated approach than previous attempts [2, 26]. If not carefully constructed, naive realizations of the non-convex optimization may often result in ineffective filters. There are many reasons for ending up with an inferior filter: for instance the filter may be asymmetric, be the outcome of an uncovered optimization process, or even have parameters hardly compatible with a spectrum-slicing solver. In order to yield consistent results, we provide a selection of initial parameters that consistently yield “good” filters.

Fire-and-forget optimization. We describe and discuss the choices of parameters that might lead the optimization process astray, ending up with ineffective filters. We propose a number of guidelines that consistently yield filters that work well with solvers based on the resolvent operator. In most cases no trial-and-error in the parameter selection is required. We argue at length on the principles that should guide the user in the choice of Least-Squares weights, and constraints for the optimization.

Ready-to-use SLiSe filters. In order showcase the promise of our optimization approach, we provide ready-to-use SLiSe filters. We compare such filters with existing ones using a large representative problem set. These SLiSe filters can be used as drop-in replacements for the current state-of-the-art spectrum-slicing eigensolver libraries such as FEAST.

1.1. Subspace Iteration Method Accelerated via Spectral Projection. This section presents some mathematical background on subspace iteration methods based on resolvents expressed as rational functions, the main area of application that we will consider. Our focus is on the Hermitian interior eigenvalue problem. Given a Hermitian matrix $A = A^\dagger \in \mathbb{C}^{n \times n}$ and a proper interval $[a, b]$, with $[a, b] \cap [\lambda_1, \lambda_n] \neq \emptyset$, we are interested in finding the m eigenpairs (λ, v) inside $[a, b]$ resolving the secular equation:

$$Av = \lambda v.$$

An efficient subspace iteration method necessitates a projection procedure that identifies a search subspace approximating the invariant eigenspace corresponding to the eigenvalues lying in the $[a, b]$ interval. In the course of this paper we focus solely on methods that achieve such projection through a rational function $f(A)$ of the matrix A . Such functions are also known as rational filters although other filter forms, such as polynomial filters, do exist. A rational filter of degree $(n - 1, n)$ can be expressed as a matrix function in partial fraction decomposition

$$\sum_{i=1}^n \alpha_i (A - Iz_i)^{-1} = f(A) \tag{1.1}$$

where $z_i \in \mathbb{C}$ and $\alpha_i \in \mathbb{C}$ are chosen in a way such that the eigenvalues of A inside $[a, b]$ are mapped to roughly one, and the eigenvalues outside are mapped to roughly zero. As a result, the filter suppresses eigenvalues outside of $[a, b]$, which improves convergence of the subspace iteration for the desired eigenvalues and eigenvectors. In this context f , as a scalar function, can be seen as a rational approximation to the indicator function $\chi_{[a,b]}$, with unit value inside $[a, b]$ and zero everywhere else. Filters are usually generated for a search interval of $[-1, 1]$ and then mapped to $[a, b]$ via an appropriate transformation on the α_i ’s and z_i ’s. Without loss of generality we always consider the search interval to be $[-1, 1]$. Forming $f(A)$ from Equation (1.1) explicitly involves the calculation of the matrix inverse. Using $f(A)$ within a subspace iteration procedure requires only $X := f(A)Y$, which can be rewritten as p independent linear system solves:

$$(A - Iz_i)X = \alpha_i Y \quad 1 \leq i \leq p \tag{1.2}$$

If we assume that $f(A)$ outputs a good approximation to the search subspace, a common form of subspace iteration is based on the use of the Rayleigh-Ritz (RR) projection at each iteration.

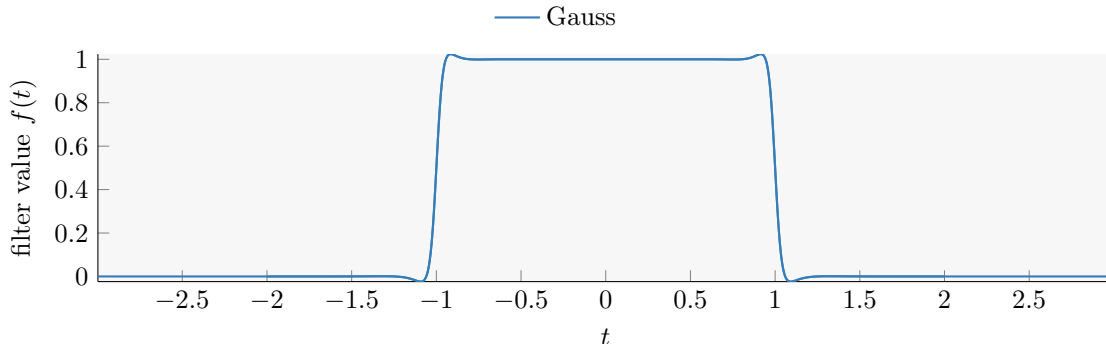


Fig. 1.1: Plot of the Gauss filter obtained by 16-points Gauss-Legendre quadrature of Equation (1.3), assuming $t \in \mathbb{R}$.

Provided that the approximating subspace has a dimension \mathbf{p} equal or larger than \mathbf{m} , such a projection reduces the size of the eigenproblem to be solved, and is guaranteed to output eigenpairs of the reduced problem that are in a one-to-one correspondence with the eigenpairs inside the search interval.

One of the most well-known solvers for the interior eigenvalue problem based on a rational resolvent followed by a the RR projection is the FEAST library [22]. FEAST derives the filter function via p -point quadrature of the contour integral:

$$\frac{1}{2\pi i} \int_{\Gamma} \frac{dt}{t - A} \approx \frac{1}{2\pi i} \sum_{i=1}^p w_i (A - Ix_i)^{-1} = f(A) \quad (1.3)$$

where Γ is a contour in the complex plane enclosing the search interval $[a, b]$. Quadrature along Γ yields integration nodes $x_i \in \mathbb{C}$ and weights $w_i \in \mathbb{C}$. While any quadrature rule can filter the eigenvalues to some extent, FEAST’s defaults to the Gauss-Legendre quadrature rules. From Equation (1.3) follows that numerical integration of the contour integral is functionally equivalent to the rational filter formulation of Equation (1.1). Accordingly, we can interpret FEAST’s filter as a rational filter with $x_i = z_i$ and $w_i = \alpha_i$; we will call the resulting filter “Gauss filter”. As we are considering Hermitian eigenproblems, we can plot the Gauss filter by considering $f(t)$ as a scalar function of $t \in \mathbb{R}$. Figure 1.1 plots the Gauss filter obtained by a 16-points quadrature on a circle-shaped contour that circumscribes $[-1, 1]$ symmetrically with respect to the real axis. The resulting function is even and real-valued on the entire real axis.

The convergence rate of the FEAST algorithm for a chosen filter f is given by [25]:

$$\tau = \frac{|f(\lambda_{\mathbf{p}+1})|}{|f(\lambda_{\mathbf{m}})|} \quad (1.4)$$

for a filter f and an ordering of the eigenvalues such that

$$|f(\lambda_1)| \geq |f(\lambda_2)| \geq \dots \geq |f(\lambda_{\mathbf{m}})| \geq \dots \geq |f(\lambda_{\mathbf{p}})| \geq \dots \geq |f(\lambda_{\mathbf{p}+1})| \geq \dots |f(\lambda_n)|.$$

For most filters it is the case that $f(1) = f(-1) = \frac{1}{2}$, in which case we can extend the above equation with: $|f(\lambda_{\mathbf{m}})| \geq \dots \geq \frac{1}{2} \geq \dots \geq |f(\lambda_{\mathbf{p}})|$.

The rest of this paper is structured as follows. To showcase the potential of our optimization method, Section 2 discusses example SLiSe filters. Section 3 considers the formulation of the non-linear Least-Squares problem. We discuss the use of symmetries of the filters, as well as the residual level function and its gradients, which also make use of these symmetries. In Section 4 we provide a full framework for the generation of SLiSe filters. Related work is presented in Section 5, and we conclude in Section 6.

2. Examples of SLiSe Filters. In this section we provide a concise illustration of the main result of the paper. Specifically, we present SLiSe filters that are meant as replacements for existing

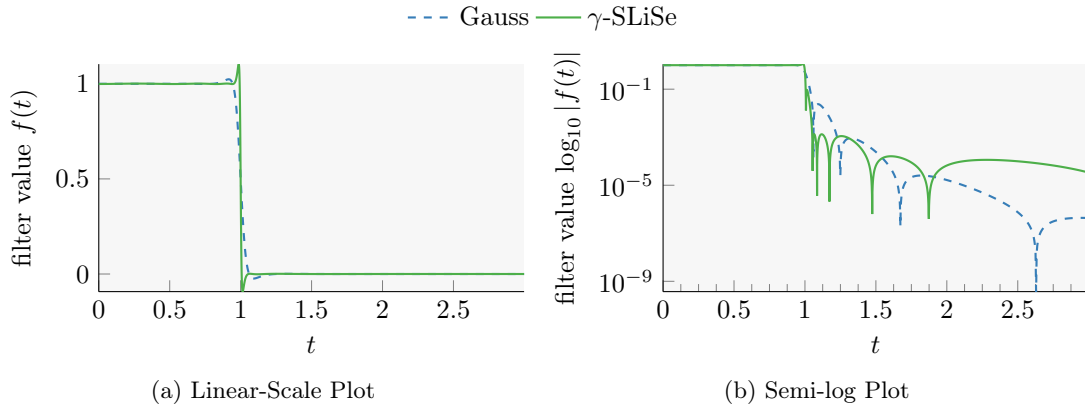


Fig. 2.2: Plots of the Gauss filter and our replacement candidate, γ -SLiSe. Both filters have 16 poles and coefficients.

a problem with m eigenpairs inside the search interval we select a size of the subspace iteration of $p = 1.5m$, the value that FEAST recommends for the Gauss filter.

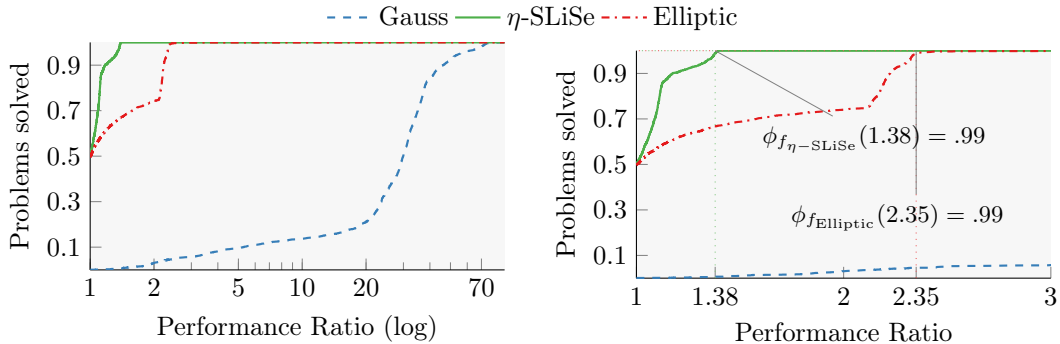
Figure 2.1a shows a histogram of the iterations required for the 2116 benchmark problems by the γ -SLiSe and the Gauss filter. Independently of which filter is used the vast majority of problems of the set requires either 3 or 4 FEAST iterations. Fast convergence of FEAST’s subspace iteration is a known feature for the Gauss filter when p is chosen large enough. When FEAST uses the γ -SLiSe filter, most benchmark problems require 3 iterations, with only some problems requiring 4 or more iterations. In contrast, when the Gauss filter is used, a larger number of problems require 4 iterations. Summing the iterations for all of the benchmark problems the γ -SLiSe filter requires 6774 iterations, while the Gauss filter requires 7119 iterations. Since every iteration requires 8 linear system solves and additional overhead, such as the calculation of the residuals, saving even a single iteration is a substantial performance improvement.

The increased performance of the γ -SLiSe filter comes with some drawbacks. On the one hand, the Gauss filter is more versatile than the γ -SLiSe. For instance, outside of the selected interval, the Gauss filter decays very quickly to low values (see Figure 2.2b), which yields better convergence when increasing the number of vectors in the subspace iterations p to a larger multiple of m . The γ -SLiSe does not have this property, and so does worse when a very large spectral gap is present. On the other hand, it is always possible to generate a different SLiSe filter that performs well also for large spectral gaps.

2.1.1. Convergence Ratio as a Means of Comparison. While Figure 2.1a shows some promise as a tool for comparing filters, the approach has a number of problems. Subspace iteration counts provide a very coarse look at the performance of a filter, underlined by the fact that most benchmark problems require a very similar number of iterations for both filters. Further, the evaluation requires the use of a linear system solver, and thus the outcome is dependent on the algorithm and the parameters used (such as the desired accuracy, the type of solver, etc.). A more reliable comparison should be based on a more fine-grained metric which does not depend on a specific solver, its specific parameters, and the computational kernels used. One such metric is the rate of convergence τ , defined in Equation (1.4), exhibited by the filters on each problem of the benchmark set. For small to medium sized problems, we can obtain all eigenvalues of the matrix and calculate the convergence rate analytically. The rate of convergence has a number of advantages over comparisons based on iteration counts. First, it does not depend on a specific solver, and it is cheaper to compute, as τ is a function of only the eigenvalues and not the entire matrix. Then for testing purposes, we can compute all eigenvalues up front, and then compute inexpensively τ for every benchmark problem.

Figure 2.1b shows the convergence rates for the same 2116 benchmarks problems as in Figure

adjusted to 10^{-13}



(a) Semi-log performance profile of the convergence rate. (b) The same performance profile zoomed into $[1, 3]$ with a linear axis

Fig. 2.3: Semi-log performance profile of the convergence rate for the Gauss, η -SLiSe, and Elliptic filters. η -SLiSe is meant to replace the Elliptic filter. All filters have 16 poles and $\mathbf{p} = \mathbf{m}$.

2.1a in a form called *performance profiles* [7]. For a filter f , and a given point x on the abscissa, the corresponding value $\phi_f(x)$ of the graph indicates that for $100 \cdot \phi_f(x)$ percent of the benchmark problems the filter f is at most a factor of x worse than the fastest of all methods in question. For example, $\phi_{f_{\text{Gauss}}}(3.4) \approx 0.88$ indicates that for 88% of the benchmark problems the Gauss filter yields either the best convergence rate or a rate that is within a factor of 3.4 from the best. So the performance profiles not only report how often a filter performs best, but also how badly the filter performs when it is not the best. We will use performance profiles multiples times in this section to compare the filters. From the value of $\phi_{f_{\gamma\text{-SLiSe}}}(1)$ in Figure 2.1b we can infer that γ -SLiSe achieves the best convergence rate for 77% of the benchmark problems, while the Gauss filter does best on the remaining 23% the problems. Moreover, the Gauss filter achieves a convergence rate that is worse than 3.4 times that of the γ -SLiSe filter for 12% of the problems $\phi_{f_{\text{Gauss}}}(3.4) \approx 0.88$. In conclusion, the SLiSe filter performs better than the Gauss filter in both metrics, iterations counts and convergence rate. However, the performance profile gives a much more detailed comparison.

Figure 2.2a plots both filter functions; only the positive part of the abscissa is shown as the functions are even. Figure 2.2b shows the absolute value of the same filter functions as a logplot. The γ -SLiSe filter performs better than the Gauss filter due to a smaller absolute value between 1.1 and 1.6 than the Gauss filter. A smaller absolute value outside the search interval—specifically for $|f(\lambda_{\mathbf{p}+1})|$ —improves the convergence rate τ . We set \mathbf{p} to the recommended value of $1.5\mathbf{m}$. A roughly equidistant spacing of the eigenvalues around the canonical search interval $[-1, 1]$ yields $\lambda_{\mathbf{p}+1} \approx \pm 1.25$. The γ -SLiSe filter out-performs the state-of-the-art Gauss filter for $\lambda_{\mathbf{p}+1} \in [1.1, 1.6]$. If either end of the search interval is near a large spectral cluster then $\lambda_{\mathbf{p}+1} \ll 1.1$, and neither of the two filters will do particularly well. In such a case a larger \mathbf{p} is chosen, or Elliptic filters are used. We present the Elliptic filter—and a SLiSe filter meant to replace it—in the next subsection.

2.2. η -SLiSe: A Replacement Candidate for the Elliptic Filter. The Elliptic filter, also called Caue or Zolotarev filter, has been proposed for use in the context of the interior eigenvalue problem in a number of publications [8, 17–21]². This filter is used specifically when large spectral clusters are at or near the endpoints of a search interval. In these cases the Gauss filter exhibits very slow convergence unless \mathbf{p} is chosen much larger than $1.5\mathbf{m}$. We propose η -SLiSe as a replacement for the Elliptic filter currently used in contour-based subspace iteration methods.

The Elliptic filter is an optimal filter, in the sense that the filter function is the best uniform rational approximation of the indicator function. Such a filter is worst-case optimal with respect to the convergence rate of Equation (1.4), for a subspace size of $\mathbf{p} = \mathbf{m}$. In simple terms, the Elliptic filter works better than the Gauss filter in the presence of spectral clusters close to the interval

²Technically the Elliptic filter is a class of filters depending on a number of paramters, we consider the specific filter discussed in [8]

boundary because it drops from 1 to 0 more quickly. The η -SLiSe filter trades off a slightly larger absolute values inside $[1, 1.01]$ for smaller absolute values in $[1.01, \infty]$ ($[-1.01, 1]$ and $[-\infty, 1.01]$, respectively). In Section 4.6 we elaborate on the choice of optimization parameters that yield the η -SLiSe filter.

Figure 2.3 shows a performance profile of the convergence rate for the Gauss, η -SLiSe, and Elliptic filters. Figure 2.3a is a semi-log plot of the performance profile, while Figure 2.3b is a linear-scale plot, zoomed into the interval $[1, 3]$. The comparison between the two filters needs to be adjusted to represent the specific use case of spectral clusters near the endpoints. We reuse the 2116 benchmark problems from the ‘‘Si2’’ matrix from the previous comparison, however, instead of target subspace size of $\mathbf{p} = 1.5\mathbf{m}$, we choose $\mathbf{p} = \mathbf{m}$. Thus, the eigenvalue of largest absolute function value outside the search interval determines convergence for all benchmark problems. For large spectral clusters $|f(\lambda_{\mathbf{p}+1})|$ is likely to be close to $|f(\lambda_{\mathbf{m}})|$, so this metric serves as an estimator of the filter’s behaviour with spectral clusters near the endpoints of the search interval.

The figure indicates that, for our representative set of benchmark problems, the η -SLiSe filter displays better convergence rates than the Elliptic filter. The Elliptic filter achieves the best convergence ratio for half of the benchmark problems, and η -SLiSe does it for the other half. Further, the figure indicates that for 99% of the problems, the Elliptic filter exhibits a convergence ratio within a larger factor from the convergenc ratio of η -SLiSe with $\phi_{f_{\text{Elliptic}}}(2.35) = .99$, and $\phi_{f_{\eta\text{-SLiSe}}}(1.38) = .99$ respectively. That is, for 99% of the problems η -SLiSe performs within a factor of 1.38 of the convergence ratio of the Elliptic filter. Simply put, η -SLiSe performs better than the Elliptic filter for half of the problems, and for the other half it performs very similar to the Elliptic filter. Conversely, the Elliptic filter exhibits convergence rates for some problems that are twice as bad as the convergence rate of η -SLiSe. The Gauss filter exhibits the worst rates of convergence by far, but this is to be expected as the Gauss filter is not meant for this use-case.

3. Rational Filters for Hermitian Operators: A Non-Linear Least-Squares Formulation. Before discussing the actual optimization, we need to reformulate the mathematical problem. Rational filters can be written as a sum of simple rational functions ϕ_i

$$f(t, z, \alpha) = \sum_{i=1}^n \phi_i \equiv \sum_{i=1}^n \frac{\alpha_i}{(t - z_i)} \quad (3.1)$$

with $z_i, \alpha_i \in \mathbb{C}$. We restrict ourselves to the case where the z_i and the α_i are pair-wise distinct, and the z_i have non-zero real and imaginary parts. Our initial goal is to set the stage for the formulation of a reliable method dictating the choice for the poles z_i and the coefficients α_i such that $f(t)$ constitutes an effective and flexible approximation to the ideal filter $h(t)$. In the Hermitian case such an ideal filter corresponds to the indicator function defined as

$$h(t) = \chi_{[-1,1]} = \begin{cases} 1 & \text{if } -1 \leq t \leq 1 \\ 0 & \text{otherwise} \end{cases} . \quad (3.2)$$

As $h(t)$ is discontinuous we have to specify in what sense a given filter $f(t, z, \alpha)$ is close to the target function $h(t)$. To this end, we focus on the squared difference of $h(t) - f(t, z, \alpha)$ with respect to the L_2 norm which is equivalent to defining a Least-Squares error function, or *residual level function*

$$F(z, \alpha) = \|h - f(z, \alpha)\|_2^2. \quad (3.3)$$

An optimal filter, in this sense, is the minimizer of the residual level function

$$\min_{\alpha_i, z_i} \int_{-\infty}^{\infty} \mathfrak{G}(t) \left| h(t) - \sum_{i=1}^n \frac{\alpha_i}{(t - z_i)} \right|^2 dt, \quad (3.4)$$

resulting in a weighted Least-Squares optimization problem with the weight function $\mathfrak{G}(t)$. In order to simplify the optimization process we impose the following restrictions on the weight function: 1)

$\mathfrak{G}(t)$ is piece-wise constant with bounded interval endpoints, 2) the number of piece-wise constant parts is finite, 3) the weight function is even: $\mathfrak{G}(t) = \mathfrak{G}(-t)$.

In Section 3.1 we illustrate how to exploit the symmetries of the indicator function $h(t)$ in the Hermitian case. The rational function $f(t)$ approximating $h(t)$ can be constructed so as to explicitly satisfy these symmetries, which limits the degrees of freedom used in the optimization problem. Section 3.2 contains a formulation of the Least-Squares residual level function, while its gradients are introduced in Section 3.3.

3.1. Discrete Symmetries of the Rational Approximant. We wish to construct a rational function $f(t, z, \alpha)$ that explicitly preserves the symmetries of the target function $h(t)$. The target function is invariant under two symmetry transformations, namely *complex conjugation*, and *reflection*. The first symmetry seems trivial since h is real-valued but f in general is not. The second symmetry states that h is even. For the rational function f to be a good approximation of h it should satisfy both symmetries

$$\begin{aligned} 1. \quad \text{Complex Conjugation (C):} \quad & \bar{f}(t, z, \alpha) = f(t, z, \alpha) \\ 2. \quad \text{Reflection or Parity (P):} \quad & f(-t, z, \alpha) = f(t, z, \alpha) \end{aligned} \quad (3.5)$$

Requiring the function f to satisfy the C symmetry implies that half of the rational monomials ϕ_i s are conjugate of each other. In other words, half of the poles z_i s (and corresponding α_i s) are in the upper-half of \mathbb{C} (indicated as \mathbb{H}^+) with the other half in the lower-half (\mathbb{H}^-). Then, without loss of generality we can enumerate the ϕ_i such that the first $p = \frac{n}{2}$ have poles z_i in \mathbb{H}^+ : $\frac{\alpha_r}{t-z_r} = \phi_r = \bar{\phi}_{r+p}$ with $z_r \in \mathbb{H}^+$ for $1 \leq r \leq p$. This conclusion enables us to rewrite the sum over monomials ϕ_i as a sum over half the index range $1 \leq j \leq p = \frac{n}{2}$

$$f(t, v, \beta) = \sum_{j=1}^p (\psi_j + \bar{\psi}_j) \equiv \sum_{j=1}^p \left[\frac{\beta_j}{(t-v_j)} + \frac{\bar{\beta}_j}{(t-\bar{v}_j)} \right], \quad (3.6)$$

where we relabeled the poles z_i s, the coefficients α_i s, and the monomials ϕ_i s to make the symmetry explicit.

$$\begin{aligned} z_j &= v_j & \alpha_j &= \beta_j & \phi_j &= \psi_j \\ z_{j+p} &= \bar{v}_j & \alpha_{j+p} &= \bar{\beta}_j & \phi_{j+p} &= \bar{\psi}_j \end{aligned} \quad (3.7)$$

Notice that satisfying the C symmetry forces the association of conjugate coefficients $\bar{\beta}_j$ with conjugate poles \bar{v}_j .

Imposing the P symmetry explicitly is a bit more tricky. It can be visualized as a symmetry for the complex numbers v_j, β_j and their conjugates, living in the complex plane. Consider the poles v_k in the right (R) upper-half of the complex plane \mathbb{H}^{+R} , that is those v_k with $\Re(v_k) > 0$ and $\Im(v_k) > 0$. Let the number of v_k in \mathbb{H}^{+R} be q . Applying the P symmetry to the monomials ψ_k with poles v_k in \mathbb{H}^{+R} yields:

$$\psi_k(t, v, \beta) = \frac{\beta_k}{(t-v_k)} \rightarrow -\frac{\beta_k}{(t+v_k)} = \psi_k(t, -v, -\beta)$$

Consequently the reflection operation maps a rational monomial with a pole in \mathbb{H}^{+R} to a monomial with a pole in \mathbb{H}^{-L} . For f to be invariant under reflection, the q ψ_j monomials with poles in \mathbb{H}^{+R} “must” map to the $\bar{\psi}_j$ monomials with poles in \mathbb{H}^{-L} . By complex conjugation, these same q ψ_j monomials map to $\bar{\psi}_j$ monomials in \mathbb{H}^{-R} , consequently $p = 2q$. Now we can enumerate the monomials such that the first half of ψ_j are in \mathbb{H}^{+R} , the second half of ψ_j are in the \mathbb{H}^{+L} , the first half of $\bar{\psi}_j$ are in \mathbb{H}^{-R} and the last q $\bar{\psi}_j$ are in \mathbb{H}^{-L} . Invariance under reflection implies then that $\psi_k(t, -v, -\beta) = \bar{\psi}_{k+q}(t, \bar{v}, \bar{\beta})$ for $1 \leq k \leq q$. The same reasoning can be repeated for monomials ψ_k in \mathbb{H}^{+L} . Finally, we can express f by summing over a reduced range $1 \leq k \leq q$ as

$$f(t, w, \gamma) = \sum_{k=1}^q (\chi_k + \bar{\chi}_k + \chi_k^\pi + \bar{\chi}_k^\pi) = \sum_{k=1}^q \left[\frac{\gamma_k}{t-w_k} + \frac{\bar{\gamma}_k}{t-\bar{w}_k} - \frac{\gamma_k}{t+w_k} - \frac{\bar{\gamma}_k}{t+\bar{w}_k} \right]. \quad (3.8)$$

Once again, we have relabeled poles, coefficients, and monomials so as to make explicit the symmetry indicated by the π symbol

$$\begin{aligned} v_k &= w_k & \beta_k &= \gamma_k & \psi_k &= \chi_k \\ v_{k+q} &= \bar{w}_k^\pi = -\bar{w}_k & \beta_{k+q} &= \bar{\gamma}_k^\pi = -\bar{\gamma}_k & \psi_{k+q} &= \bar{\chi}_k^\pi \\ \bar{v}_k &= \bar{w}_k & \bar{\beta}_k &= \bar{\gamma}_k & \bar{\psi}_k &= \bar{\chi}_k \\ \bar{v}_{k+q} &= w_k^\pi = -w_k & \bar{\beta}_{k+q} &= \gamma_k^\pi = -\gamma_k & \bar{\psi}_{k+q} &= \chi_k^\pi \end{aligned} \quad (3.9)$$

We would have reached the same result if we started to require invariance under the symmetries in reverse order³.

3.2. Residual Level Function. Let us expand Equation (3.3) by temporarily disregarding the discrete symmetries of the rational function and expressing f as in Equation (3.1)

$$\begin{aligned} F(z, \alpha) &= \|h - \sum_i \alpha_i \phi_i\|_2^2 \\ &= \langle h - \sum_i \alpha_i \phi_i, h - \sum_i \alpha_i \phi_i \rangle \\ &= \langle h, h \rangle - \langle h, \sum_j \alpha_j \phi_j \rangle - \langle \sum_i \alpha_i \phi_i, h \rangle + \langle \sum_i \alpha_i \phi_i, \sum_j \alpha_j \phi_j \rangle \\ &= \langle h, h \rangle - 2\Re[\sum_i \langle \phi_i, h \rangle \alpha_i] + \sum_i \sum_j \bar{\alpha}_i \alpha_j \langle \phi_i, \phi_j \rangle. \end{aligned}$$

The residual level function is expressible as

$$F(z, \alpha) = \alpha^\dagger G \alpha - 2\Re[\eta^\dagger \alpha] + \|h\|^2 \quad (3.10)$$

where the $x^\dagger \equiv \bar{x}^\top$ indicates complex conjugation plus transposition (Hermitian conjugation) and

$$G_{ij} = \langle \phi_i, \phi_j \rangle, \quad \eta_i = \langle \phi_i, h \rangle.$$

The inner products $\langle \cdot, \cdot \rangle$ are defined through a weight function $\mathfrak{G}(t)$

$$\langle \phi_i, \phi_j \rangle = \int_{-\infty}^{+\infty} \mathfrak{G}(t) \bar{\phi}_i(t) \phi_j(t) dt = \int_{-\infty}^{+\infty} \frac{\mathfrak{G}(t)}{(t - \bar{z}_i)(t - z_j)} dt, \quad (3.11)$$

and

$$\eta_i = \langle \phi_i, h \rangle = \int_{-\infty}^{+\infty} \frac{\mathfrak{G}(t) h(t)}{t - \bar{z}_i} dt \quad \|h\|^2 = \int_{-\infty}^{+\infty} \mathfrak{G}(t) h(t)^2 dt.$$

We could have started directly with the CP invariant formulation from Equation (3.8) of the rational function f . We preferred this approach in order to show how requiring each symmetry to be satisfied has direct consequences on the structure of the matrix G and vector η . Recall from Equation (3.7) how the z_i s and α_i s were mapped to v_j s and β_j s so as to make explicit the C symmetry. Due to such map, the residual level function has the following block structure:

$$F = (\beta^\dagger \quad \beta^\top) \begin{pmatrix} A & B \\ B & A \end{pmatrix} \begin{pmatrix} \beta \\ \beta \end{pmatrix} - 2\Re \left[(\zeta^\dagger \quad \zeta^\top) \begin{pmatrix} \beta \\ \beta \end{pmatrix} \right] + \|h\|^2 \quad (3.12)$$

with

$$\begin{aligned} A_{i,j} &= \int_{-\infty}^{+\infty} \frac{\mathfrak{G}(t)}{(t - \bar{v}_i)(t - v_j)} dt & \zeta_i &= \int_{-\infty}^{+\infty} \frac{\mathfrak{G}(t) h(t)}{t - \bar{v}_i} dt \\ B_{i,j} &= \int_{-\infty}^{+\infty} \frac{\mathfrak{G}(t)}{(t - \bar{v}_i)(t - \bar{v}_j)} dt & B_{i,i} &= \int_{-\infty}^{+\infty} \frac{\mathfrak{G}(t)}{(t - \bar{v}_i)^2} dt \end{aligned}$$

³Physicists refer to the combination of these two discrete symmetries as CP invariance. A necessary condition for its existence is that the operators generating the transformations must commute.

for $i, j = 1, \dots, p$. The matrix A is Hermitian while B is symmetric (complex), so that $\bar{B} = B^\dagger$. This equation can be reduced since it contains only half of the unknowns as the initial residual level function. For example $\beta^\dagger \bar{A} \bar{\beta} = \beta^\dagger A \beta$ and $\beta^\dagger B \bar{\beta} = \overline{(\beta^\dagger \bar{B} \beta)}$, so that

$$(\beta^\dagger \quad \beta^\dagger) \begin{pmatrix} A & B \\ B & A \end{pmatrix} \begin{pmatrix} \beta \\ \bar{\beta} \end{pmatrix} = 2 [\beta^\dagger A \beta + \Re e (\beta^\dagger B \bar{\beta})]$$

and similarly $\zeta^\dagger \beta = \overline{\zeta^\dagger \bar{\beta}}$. With the simplifications above the residual level function reduces to

$$F(v, \beta) = \beta^\dagger A \beta + \Re e (\beta^\dagger B \bar{\beta}) - 2 \Re e (\zeta^\dagger \beta) + \frac{1}{2} \|h\|^2. \quad (3.13)$$

Now we can require the latter equation to satisfy the reflection symmetry P. Equation (3.9) maps poles v_j and coefficients β_j respectively to w_k and γ_k , so as to make the reflection symmetry explicit. The residual level function now takes on a new block form

$$F = (\gamma^\dagger \quad (\gamma^\pi)^\dagger) \begin{pmatrix} X & Y \\ Y^\dagger & X^\pi \end{pmatrix} \begin{pmatrix} \gamma \\ \bar{\gamma}^\pi \end{pmatrix} + \Re e \left[(\gamma^\dagger \quad (\gamma^\pi)^\dagger) \begin{pmatrix} W & Z \\ Z^\dagger & W^\pi \end{pmatrix} \begin{pmatrix} \bar{\gamma} \\ \gamma^\pi \end{pmatrix} \right] - 2 \Re e \left[(\theta^\dagger \quad (\theta^\pi)^\dagger) \begin{pmatrix} \gamma \\ \bar{\gamma}^\pi \end{pmatrix} \right] + \frac{1}{2} \|h\|^2 \quad (3.14)$$

with

$$\begin{aligned} W_{k,\ell} &= \int_{-\infty}^{+\infty} \frac{\mathfrak{G}(t)}{(t - \bar{w}_k)(t - \bar{w}_\ell)} dt & \bar{W}_{k,\ell}^\pi &= \int_{-\infty}^{+\infty} \frac{\mathfrak{G}(t)}{(t + w_k)(t + w_\ell)} dt \\ X_{k,\ell} &= \int_{-\infty}^{+\infty} \frac{\mathfrak{G}(t)}{(t - \bar{w}_k)(t - w_\ell)} dt & \bar{X}_{k,\ell}^\pi &= \int_{-\infty}^{+\infty} \frac{\mathfrak{G}(t)}{(t + w_k)(t + \bar{w}_\ell)} dt \\ Y_{k,\ell} &= \int_{-\infty}^{+\infty} \frac{\mathfrak{G}(t)}{(t - \bar{w}_k)(t + \bar{w}_\ell)} dt & Z_{k,\ell} &= \int_{-\infty}^{+\infty} \frac{\mathfrak{G}(t)}{(t - \bar{w}_k)(t + w_\ell)} dt \\ \theta_k &= \int_{-\infty}^{+\infty} \frac{\mathfrak{G}(t)h(t)}{t - \bar{w}_k} dt & \bar{\theta}_k^\pi &= \int_{-\infty}^{+\infty} \frac{\mathfrak{G}(t)h(t)}{t + w_k} dt \end{aligned}$$

for $k, \ell = 1, \dots, q$. These submatrix blocks preserve some of the properties of the matrix they are part of. For instance, $X^\dagger = X$ and $\bar{W} = W^\dagger$ while the P symmetry imposes new equalities $Y^\dagger = \bar{Y}^\pi$ and $Z^\dagger = \bar{Z}^\pi$. In addition to these, the P symmetry allows for additional equalities thanks to the symmetric integration boundaries of the inner product $\langle \cdot, \cdot \rangle$. In other words

$$\begin{aligned} \int_0^a g(t, w_k) dt &= \int_{-a}^0 g^\pi(t, w_k) dt & \text{for } g \text{ an even function of } t \\ \int_0^a g(t, w_k) dt &= - \int_{-a}^0 g^\pi(t, w_k) dt & \text{for } g \text{ an odd function of } t. \end{aligned}$$

The direct implication of this observation is that, for instance, $X = X^\pi$, $W = W^\pi$.

If we expand the matrix expression for the residual level function and exploit all the symmetries the final expression for F becomes

$$F = \gamma^\dagger X \gamma + (\gamma^\dagger X \gamma)^\dagger - 2 \Re e (\gamma^\dagger Y \bar{\gamma}) + \Re e \left[\gamma^\dagger W \bar{\gamma} + (\gamma^\dagger W \bar{\gamma})^\dagger - 2 \gamma^\dagger Z \gamma \right] - 2 \Re e (\theta^\dagger \gamma - (\theta^\pi)^\dagger \bar{\gamma}) + \frac{1}{2} \|h\|^2. \quad (3.15)$$

Despite the apparent complexity of the expression above, it would have been quite more complex if we started to compute the residual level function directly from Equation (3.8); the quadratic term in γ s alone would have accounted for 16 terms. Moreover the expression is a function of only γ_k s and their conjugates. Z and Y matrices appear only once, while X and W can be transformed after their computation.

3.3. Gradient of the Residual Level Function. Most optimization methods—including all the ones that we consider—require the gradient of the residual level function. We could compute the gradients analytically by using the expression for F derived in Equation (3.10). A simpler way is to compute ∇f out of the formulation in Equation (3.1) in conjunction with the formulation of F in terms on inner products $\langle \cdot, \cdot \rangle$

$$\nabla F = \nabla \langle h - f, h - f \rangle = -\langle \nabla f, h - f \rangle - \langle h - f, \nabla f \rangle = 2[\langle f, \nabla f \rangle - \langle h, \nabla f \rangle]. \quad (3.16)$$

Since $\bar{f} = f$ and the ∇ operator acts on the whole inner products, the quantities $\langle \nabla f, f \rangle$ and $\langle f, \nabla f \rangle$, while formally different, are actually the same. In addition, the gradient of a real function with respect to the conjugate of a complex variable is necessarily the conjugate of the gradient with respect to variable itself: $\nabla_{\bar{z}} f = \frac{\partial f}{\partial \bar{z}} = \frac{\partial \bar{f}}{\partial z} = \overline{\nabla_z f}$. Consequently we do not need to explicitly compute the gradient with respect the conjugate of the poles and the coefficients. Equation (3.16) can be written making explicit use of the C-symmetric or the full CP-symmetric formulation of f , which is Equations (3.6) and (3.8) respectively.

C symmetry – Let us first derive f with respect to v_k and β_k

$$\frac{\partial f}{\partial v_k} = \frac{\beta_k}{(t - v_k)^2} \quad ; \quad \frac{\partial f}{\partial \beta_k} = \frac{1}{(t - v_k)}.$$

The expression above is the k^{th} -component of the gradients $\nabla_v f$ and $\nabla_\beta f$ respectively. Plugging them in Equation (3.16) and separating terms, we arrive at the matrix expressions

$$\nabla_v F = 2 [\beta^\dagger \nabla A + \beta^\top \nabla \bar{B} - \nabla \zeta^\dagger] I_\beta \quad (3.17)$$

$$\nabla_\beta F = 2 [\beta^\dagger A + \beta^\top \bar{B} - \zeta^\dagger] \quad (3.18)$$

where A , \bar{B} and ζ are the same quantities defined in Section 3.2, while remaining matrices are defined for $i, j = 1, \dots, p$:

$$\begin{aligned} \nabla A_{i,j} &= \int_{-\infty}^{+\infty} \frac{\mathfrak{G}(t)}{(t - \bar{v}_i)(t - v_j)^2} dt & \nabla \zeta_i &= \int_{-\infty}^{+\infty} \frac{\mathfrak{G}(t)h(t)}{(t - \bar{v}_i)^2} dt \\ \nabla \bar{B}_{i,j} &= \int_{-\infty}^{+\infty} \frac{\mathfrak{G}(t)}{(t - v_i)(t - v_j)^2} dt & I_\beta &= \text{Diag}(\beta) \end{aligned}$$

CP symmetry – Analogously to what done in the C-symmetric case, we first compute the derivatives of f with respect to the poles and the coefficients

$$\frac{\partial f}{\partial w_k} = \gamma_k \left[\frac{1}{(t - w_k)^2} + \frac{1}{(t + w_k)^2} \right] \quad ; \quad \frac{\partial f}{\partial \gamma_k} = \frac{1}{(t - w_k)} - \frac{1}{(t + w_k)}.$$

After entry-wise substitution of the above components of $\nabla_w F$ and $\nabla_\gamma F$, some tedious rearrangement, and using the parity with respect to the integration limits, we arrive at the following matrix equations

$$\nabla_w F = 4 [\gamma^\dagger (\nabla X - \nabla Z) + \gamma^\top (\nabla \bar{W} - \nabla \bar{Y}) - \nabla \theta^\dagger] I_\gamma \quad (3.19)$$

$$\nabla_\gamma F = 4 [\gamma^\dagger (X - Z) + \gamma^\top (\bar{W} - \bar{Y}) - \theta^\dagger]. \quad (3.20)$$

The matrices not previously introduced are defined as follows. For $k, \ell = 1, \dots, q$:

$$\begin{aligned} \nabla X_{k,\ell} &= \int_{-\infty}^{+\infty} \frac{\mathfrak{G}(t)}{(t - \bar{w}_k)(t - w_\ell)^2} dt & \nabla Z_{k,\ell} &= - \int_{-\infty}^{+\infty} \frac{\mathfrak{G}(t)}{(t - \bar{w}_k)(t + w_\ell)^2} dt \\ \nabla \bar{W}_{k,\ell} &= \int_{-\infty}^{+\infty} \frac{\mathfrak{G}(t)}{(t - w_k)(t - w_\ell)^2} dt & \nabla \bar{Y}_{k,\ell} &= - \int_{-\infty}^{+\infty} \frac{\mathfrak{G}(t)}{(t - w_k)(t + w_\ell)^2} dt \\ \nabla \bar{\theta}_k &= \int_{-\infty}^{+\infty} \frac{\mathfrak{G}(t)h(t)}{(t - w_k)^2} dt & I_\gamma &= \text{Diag}(\gamma) \end{aligned}$$

Notice that, in both C-symmetric and CP-symmetric cases, the gradients are row vectors. While this is an arbitrary choice, it is a quite natural one to make. Moreover we decided to maintain the overall multiplicative factor in front of them; such a factor was scaled out of F when writing this in a symmetry transparent form. Once again this an arbitrary choice since re-scaling the gradient of F does not influence the minimization process.

4. Optimizing Rational Filters for Hermitian Operators. With the formulation of the residual level function and its gradient from the previous section, we can now proceed to optimize the SLiSe filters. Our goal is to minimize the residual level function F . However, there are a number of possible approaches to the minimization problem. Starting at a given position $x^{(0)}$, *descent methods* minimize $F(x)$ by iteratively refining this position, such that $F(x^{(k+1)}) \leq F(x^{(k)})$. Using the CP symmetries the minimization problem can be stated as

$$\min_x F(x) = \min_x \|h - f(w, \gamma)\|_2^2, \quad (4.1)$$

with the initial choice of parameters, or *starting position*, of the form $x^{(0)} = [w^{(0)} \ \gamma^{(0)}] = [w_1^{(0)}, \dots, w_q^{(0)}, \gamma_1^{(0)}, \dots, \gamma_q^{(0)}]$.

In Section 4.1 we present a first method to minimize Equation (4.1). Section 4.2 introduces the Levenberg-Marquardt method, a more sophisticated solver for Least-Squares problems. $F(x)$ is non-convex in the poles w of the filter function and thus a local minimum x^* is not guaranteed to be a global minimum. Depending on the starting position, descent methods, including the Levenberg-Marquardt method, may produce results that are far from globally optimal. Section 4.3 deals with the choice of the starting position in a way that mitigates this problem. We address the choice of weight function for the Least-Squares optimization in Section 4.4. In some cases it is advantageous to optimize more than just the squared differences between the filter and the indicator function $h(t)$; Section 4.5 delves into constrained optimization. Section 4.6 concludes with a discussion of a variety of SLiSe filters obtainable with the methods we discuss throughout this section.

There are alternative approaches to the optimization problem. A very different method is Branch and Bound (B&B) which, if successful, finds the global minimum. However, B&B requires a convex underestimation of the objective function instead of the gradient. We will not consider this method for two reasons. First, its success highly depends on the ability of finding a suitable underestimation, which is not an easy task. Second, B&B usually is computationally more expensive than the methods we present. Since our goal is to generate filters on the fly, we focus on cheaper methods.

4.1. Optimization via Gradient Descent. In this section we remark, through an illustrative example, on a number of issues of the optimization process, which we use to formulate some significant guidelines that are illustrated in the following sections. The most basic descent method is *gradient descent*. A gradient descent step drives down the residual level function, at the current position, along a direction collinear with its negative gradient. Given some mild assumptions, one eventually arrives at a local minimum. For a given starting position $x^{(0)}$ the update step of the gradient descent method is

$$x^{(k+1)} = x^{(k)} + s \cdot \Delta x^{(k)} = x^{(k)} - s \cdot \nabla_x F(x) \Big|_{x=x^{(k)}}, \quad s \geq 0. \quad (4.2)$$

There are number of ways to select the *step-length* s in Equation (4.2). While it is possible to set s as constant, we can improve the convergence of the method by approximating $s^{(k)} = \operatorname{argmin}_{1 \geq u \geq 0} F(x^{(k)} + u \cdot \Delta x^{(k)})$ at each iteration. To this end, we use a backtracking line search [4]: s is initialized at each step with $s = 1$ and then s is halved until $F(x + \Delta x) < F(x) + \frac{s}{2} \nabla_x F(x)^\dagger \Delta x$.

4.1.1. An Example. In the following, we present three filters obtained using the gradient descent method. The real and imaginary part of the poles w and coefficients γ of the starting positions were chosen uniformly random between $[-1, 1]^4$. For each filter function $q = 2$, and so

⁴The Least-Squares weights used to obtain these results are 1.0 inside $[-1000, 1000]$ and 0.0 everywhere else.

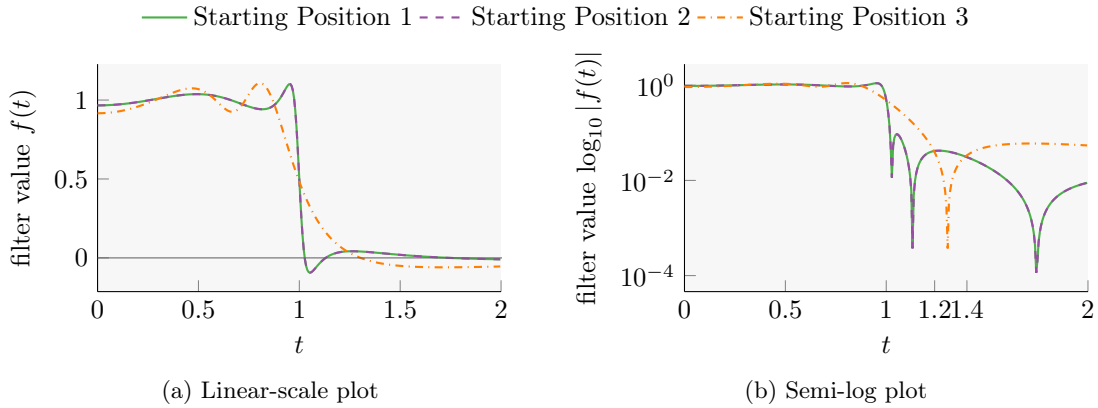


Fig. 4.1: Left side: Three SLiSe filters obtained from gradient descent with different starting positions. Right side: Semi-log plot with absolute value of the filter functions. The poles and residuals of the functions are listed in Table 4.1.

	Starting Position 1	Starting Position 2	Starting Position 3
w_1	$+0.997360 + 0.044537i$	$+0.721876 + 0.550662i$	$-0.742834 + 0.246735i$
w_2	$+0.721876 + 0.550662i$	$+0.997360 + 0.044537i$	$+0.744336 + 0.212182i$
γ_1	$-0.024019 - 0.002516i$	$-0.135117 - 0.148326i$	$+0.791429 - 0.331455i$
γ_2	$-0.135117 - 0.148326i$	$-0.024019 - 0.002516i$	$+0.639334 + 0.196414i$
$F([w \ \gamma])$	0.005846	0.005846	0.033640

Table 4.1: Poles, coefficients, and residual levels of the filter functions show in Figure 4.1

the filters have a total of 8 poles and coefficients. Using the symmetries described in Section 3.1, we need to optimize only w_1, w_2, γ_1 , and γ_2 . The three filters are plotted on semi-log scale and on a normal scale on the right hand side and the left hand side of Figure 4.1 respectively. Table 4.1 shows the poles, coefficients, and residual levels of the resulting filter functions. Starting Position 1 and 2 end in the same filter. Starting Position 3 generates a different filter with a residual level that is one order of magnitude higher than the others. As the semi-log plot shows, this last filter will likely perform significantly worse than the first two. This can be understood by noticing that the filters obtained from Starting Position 1 and 2 have a smaller absolute value in $[1, 1.21]$ and—not fully visible in the plot— $[1.4, \infty]$. From this simple example and many others we have run, we can comment on a number of undesirable properties of the gradient descent method:

REMARK 1 (Slow convergence). *Gradient descent is a fairly slow method, with linear convergence behavior at best. Even when equipped with a line-search the number of iterations required to reach a minimum is often in the millions. We see in Section 4.2 how convergence can be substantially improved by switching to a more advanced Least-Squares optimization method.*

REMARK 2 (Dependence on starting position). *The filter obtained from the optimization depends on the starting position $x^{(0)}$. Different starting positions can result in very different filters with different residual levels. Our experiments indicate that when increasing q the optimization finds more and more local minima, and their residual levels compared to the best known solutions get worse. Ideally, we want a method allowing us to choose the starting position in a manner that consistently yields good results. In Section 4.3 we discuss an approach to choosing the starting position which mitigates this problem.*

REMARK 3 (Lack of flexibility). *In order to obtain filters with distinct properties we need to modify the optimization process accordingly. Section 4.4 outlines a number of criteria for choosing the Least-Squares weight function $\mathfrak{G}(t)$. Furthermore, out-of-the-box gradient descent does not*

support constrained optimization. In Section 4.5 we illustrate a number of ways to use optimization constraints on filters.

4.2. Improving Convergence Speed. We address Remark 1 by introducing the Levenberg-Marquardt method [14, 16] (LM). This is a solver for non-linear Least-Squares problems with a better convergence rate than gradient descent. LM is an hybrid of the gradient descent and the Gauss-Newton method (a good description of both methods can be found in [15]). We present the Gauss-Newton method first, then introduce the LM method. We give a formulation based on the inner product presented in Equation (3.11).

For the sake of clarity, we re-write the residual level function in terms of $\xi([\alpha z], t) = h(t) - f(t, z, \alpha)$

$$F(x) = \|\xi(x)\|_2^2 = \langle \xi(x), \xi(x) \rangle = \int_{-\infty}^{\infty} \mathfrak{G}(t) |\xi(x, t)|^2 dt = \int_{-\infty}^{\infty} \mathfrak{G}(t) |h(t) - f(t, z, \alpha)|^2 dt,$$

where we indicate the collection of parameters $[z \ \alpha]$ with x . The basis of the Gauss-Newton method is a linear approximation of ξ

$$\xi(x + \Delta x) = \xi(x) + \nabla \xi(x) \cdot \Delta x \doteq \xi + \sum_i \frac{\partial \xi}{\partial x_i} \Delta x_i \quad (4.3)$$

which, in the following, we refer to with the shortcut notation $\xi + \nabla \xi \cdot \Delta x$. The Levenberg-Marquardt method aims at minimizing a linear approximation of the residual level function by Gauss-Newton iterates. By using the linear approximation of ξ , such a requirement can be formulated as the minimization of the following function with respect to Δx

$$\begin{aligned} F(x + \Delta x) &= \|\xi(x + \Delta x)\|_2^2 = \langle \xi, \xi \rangle + 2\langle \xi, \nabla \xi \cdot \Delta x \rangle + \langle \nabla \xi \cdot \Delta x, \nabla \xi \cdot \Delta x \rangle \\ &= F(x) + \nabla F(x) \cdot \Delta x + (\Delta x)^\dagger \cdot \langle \nabla \xi, \nabla \xi \rangle \cdot \Delta x. \end{aligned}$$

Notice that the condition $\bar{\xi}(x + \Delta x) = \xi(x + \Delta x)$ implies that $(\Delta x)^\dagger \cdot \bar{\nabla} \xi = \nabla \xi \cdot \Delta x$ with the consequence that $\langle \nabla \xi \cdot \Delta x, \xi \rangle = \langle \xi, \nabla \xi \cdot \Delta x \rangle$. Taking the partial derivative of $F(x + \Delta x)$ with respect to Δx and equating it to zero one gets

$$\partial_{\Delta x} F(x + \Delta x) = 2[\langle \xi, \nabla \xi \rangle + \langle \nabla \xi, \nabla \xi \rangle \cdot \Delta x] = 0$$

Using the formulation above, the Gauss-Newton method iterates over k in the following way:

1. Set: $H := \langle \nabla \xi(x^{(k)}), \nabla \xi(x^{(k)}) \rangle$
2. Solve: $H \cdot \Delta x_{GN}^{(k)} = \langle \xi(x^{(k)}), \nabla \xi(x^{(k)}) \rangle = -\frac{1}{2} \nabla F(x^{(k)})$
3. Update: $x^{(k+1)} = x^{(k)} + s \cdot \Delta x_{GN}^{(k)}$.

Here H acts as a linear approximation of the Hessian of F . Consequently, if H is well-conditioned, the Gauss-Newton method can have quadratic convergence. However, there are still scenarios where Gauss-Newton steps provide only a small improvement of the residual. In those cases it is beneficial to temporarily switch to gradient descent, even though it only has linear convergence at best. The Levenberg-Marquardt method employs a *dampening parameter* $\mu \geq 0$ to switch between the Gauss-Newton and gradient descent methods. By adding a dampening term, the second step is substituted by

$$2. \text{ Solve: } (H + \mu I) \Delta x_{LM}^{(k)} = -\frac{1}{2} \nabla F(x^{(k)}), \quad (4.4)$$

where the gradient of F is intended over both the poles and coefficients. Such an addition is equivalent to a constrained Gauss-Newton with the parameter μ working as a Lagrange multiplier.

In practice, the dampening parameter μ is re-adjusted after every iteration. For a small μ , the solution to Equation (4.4) is similar to the Gauss-Newton update step $\Delta x_{LM} \simeq \Delta x_{GN}$. On

the other hand, when μ is large then $\Delta x_{LM} \simeq -\frac{1}{\mu} \nabla F(x)$, which is similar to the gradient descent update step. Often, instead of $H + \mu I$ one uses $H + \mu \cdot \text{diag}(H)$. Generally, when a LM-step reduces the residual by a large amount, then μ is decreased. When a step does not decrease the residual, or does not reduce the residual by enough, μ is increased. So for large μ the resulting update Δx_{LM} becomes increasingly similar to the gradient descent update.

Since the formulations of the LM method given so far is independent from the symmetry of f , it is valid for any formulation of the rational filter. Let us look now more in detail at H . This is a matrix whose entries are $H_{i,j} = \langle \nabla_{x_i} f, \nabla_{x_j} f \rangle$ which, in the case of CP symmetry, can be represented in block form as

$$H = \begin{pmatrix} H_2 & -\bar{H}_1 & \bar{H}_1 & -H_2 \\ -H_1 & H_2^\dagger & -H_2^\dagger & H_1 \\ H_1 & -H_2^\dagger & H_2^\dagger & -H_1 \\ -H_2 & \bar{H}_1 & -\bar{H}_1 & H_2 \end{pmatrix}. \quad (4.5)$$

Only two of the matrix blocks composing H are independent and are made of the following sub-blocks

$$H_1 = \begin{pmatrix} \langle \nabla_w f, \nabla_w f \rangle & \langle \nabla_w f, \nabla_\gamma f \rangle \\ \langle \nabla_\gamma f, \nabla_w f \rangle & \langle \nabla_\gamma f, \nabla_\gamma f \rangle \end{pmatrix} = 2 \begin{pmatrix} I_\gamma [\nabla \nabla \bar{W} - \nabla \nabla \bar{Y}] I_\gamma & I_\gamma [\nabla \bar{W} - \nabla \bar{Y}]^\top \\ [\nabla \bar{W} - \nabla \bar{Y}] I_\gamma & \bar{W} + \bar{Y} \end{pmatrix} \quad (4.6)$$

$$H_2 = \begin{pmatrix} \langle \nabla_{\bar{w}} f, \nabla_w f \rangle & \langle \nabla_{\bar{w}} f, \nabla_\gamma f \rangle \\ \langle \nabla_{\bar{\gamma}} f, \nabla_w f \rangle & \langle \nabla_{\bar{\gamma}} f, \nabla_\gamma f \rangle \end{pmatrix} = 2 \begin{pmatrix} I_\gamma^\dagger [\bar{\nabla} \nabla X - \bar{\nabla} \nabla Z] I_\gamma & I_\gamma^\dagger [\nabla X - \nabla Z]^\dagger \\ [\nabla X - \nabla Z] I_\gamma & X - Z \end{pmatrix} \quad (4.7)$$

where the only additional matrices that need to be defined are

$$\begin{aligned} \nabla \nabla \bar{W}_{i,j} &= \int_{-\infty}^{+\infty} \frac{\mathfrak{G}(t)}{(t - w_i)^2 (t - w_j)^2} dt & \nabla \nabla \bar{Y}_{i,j} &= - \int_{-\infty}^{+\infty} \frac{\mathfrak{G}(t)}{(t - w_i)^2 (t + w_j)^2} dt \\ \bar{\nabla} \nabla X_{i,j} &= \int_{-\infty}^{+\infty} \frac{\mathfrak{G}(t)}{(t - \bar{w}_i)^2 (t - w_j)^2} dt & \bar{\nabla} \nabla Z_{i,j} &= - \int_{-\infty}^{+\infty} \frac{\mathfrak{G}(t)}{(t - \bar{w}_i)^2 (t + w_j)^2} dt. \end{aligned}$$

The factor of 2 in front of the block matrices H_1 and H_2 comes from the P symmetry in combination with the evenness of the integral boundaries (i.e. $X = X^\top$, $\nabla X = \nabla X^\top$, etc.). Notice that block rows 3 and 4 of Eq. (4.5) are exactly equivalent, up to a sign, to block rows 2 and 1 respectively. Similarly, block columns 3 and 4 are proportional to block columns 2 and 1. This is expected due to the CP symmetry. In addition, H_1 is complex symmetric ($H_1^\dagger = \bar{H}_1$), and H_2 is complex Hermitian ($H_2^\dagger = H_2$) which, implicitly, verifies that H is complex Hermitian itself.

Going back to the Equation (4.4), one can also write the vector Δx_{LM} in block notation,

$$(\Delta x_{LM})^\top = [(\Delta y)^\top - (\Delta y)^\dagger (\Delta y)^\dagger - (\Delta y)^\top]$$

with $(\Delta y)^\top = [\Delta w^\top \Delta \gamma^\top]$. Writing Equation (4.4) in terms of Δy with $\mu \cdot \text{diag}(H)$ in place of μI one obtains 4 separate equations. Thanks to the symmetries of H , it is possible to reduce them to a single equation solving for Δy . There are several different way to achieve this result. Starting from the third equation, one can extract $(H_1 \Delta y)$ as a function of H_2^\dagger , $\Delta \bar{y}$, and $\nabla_{\bar{y}} F$, then take the conjugate of it, and substitute it in the fourth equation. The final result is a linear system solves whose dimension is one fourth of the original size of H

$$[i \Im m(H_2) - \mu \text{diag}(H_2)] \Delta y = \frac{1}{2} \nabla_y F \quad (4.8)$$

The Levenberg-Marquardt method is faster than gradient descent. An improved convergence rate, together with the reduced size of the equation to be solved, substantially accelerate the time to solution. This is a critical step for being able to generate filters on the fly.

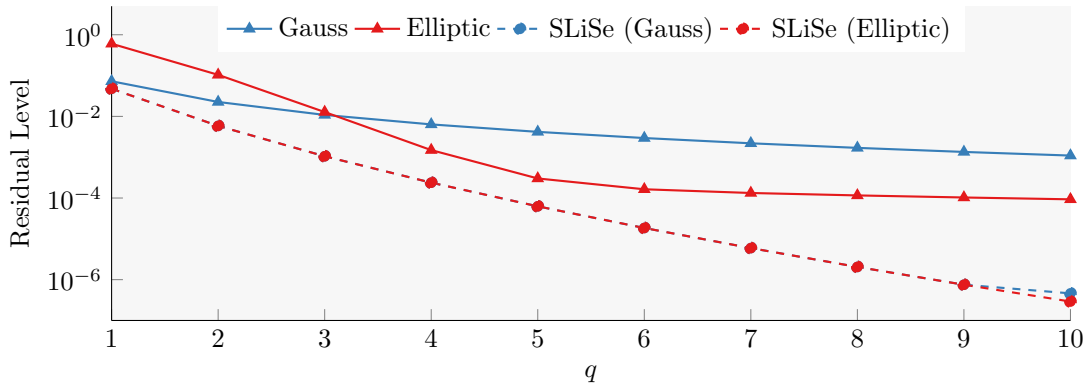


Fig. 4.2: Residual levels of Gauss and Elliptic filters, as well as, SLiSe filters obtained from Gauss and Elliptic filters as starting positions.

4.3. Systematic Choice of Starting Position. In this section we address the dependence of the optimization process on the initial conditions. In Remark 2 we pointed out that the optimized filter crucially depends on the starting position. Usually, the choice of starting positions for non-linear optimization is a difficult problem. Many heuristics exist; some methods rely on solving a convex variant of the problem [4]. Generally, it is preferable to use domain knowledge in the initial choice of starting position. Recall that the parameters of our optimization, the poles and coefficients, define a rational filter function. In general, random choices for w and γ do not produce good filters. We can reinterpret the problem of finding good starting positions for the poles and coefficients as finding a filter that serves as a good initial guess for an optimized filter. To this purpose we could use contour filters expressed through a numerical implementation of Cauchy’s Residue Theorem (see Sec.1.1), namely the Gauss and Trapezoidal filters, or more specialized ones, like the Elliptic filter, that have already been proposed as substitutes for the contour solvers [8].

To realize why the starting positions are crucial for the optimization method let us consider what happens when increasing q , the number of poles and coefficients in one quadrant of \mathbb{C} . For some spectrum slices of a given eigenvalue problem, larger values for q , say $q = 10$ or higher, may be required to obtain the desired convergence of the solver. For instance, some methods, such as the DD-PP projection method [13] that do not iterate the subspace, have little choice but to choose large q . A given value of q results in $4q$ real degrees of freedom in the optimization: q poles and q coefficients, each one with a real and imaginary part. As a result, optimization with large q becomes more and more expensive. In Figure 4.1 we have seen an example of multiple local minima of the residual level function F with $q = 2$. Our extensive numerical experiments indicate that higher q values not only increase the number of local minima in F , but have the effect of worsening the residual levels of most of these additional local minima w.r.t the best known local minimum. In one of our numerical experiments, using a random starting position with $q = 8$ yields a filter with a residual of 5.4×10^{-4} , while with $q = 4$ we achieved a residual level of 2.4×10^{-4} . Choosing $q = 8$ requires 18 linear system solves for each filter application, whereas $q = 4$ requires only 8 solves. To offset the additional cost of the linear system solves we want a filter that has a lower residual level, thus likely requiring fewer subspace iterations. Without a good starting position we obtain a filter with $q = 8$ that requires *more* linear system solves and *more* iteration. What is more, the optimization for a filter with $q = 8$ is significantly more expensive than for $q = 4$. Simply put, random starting positions yield worse and worse filters for larger q .

While choosing random starting positions does not work well with larger q , choosing existing filters produces very good results. Figure 4.2 shows the residual levels⁵ of different filters for different q . The residual levels of the Gauss filter are indicated with blue triangles, the residual levels of the Elliptic filter in red triangles. Shown with blue circles is the residual level of the filter that is obtained when the initial position of the SLiSe optimization is started with the Gauss

⁵The weight function used has unit weight between -1000 and 1000

$ t \in$	[0, .95)	[.95, .995)	[.995, 1.005)	[1.005, 1.05)	[1.05, 1.2)	[1.2, 2)	[2, 5)	[5, ∞)
$\mathfrak{G}_1(t)$	1	4	2	4	1	0	0	0
$\mathfrak{G}_2(t)$	1	4	2	4	1	.05	.001	0
$\mathfrak{G}_3(t)$	1	4	0	0	1	.2	.2	0

Table 4.2: Three separate weight functions $\mathfrak{G}_1, \mathfrak{G}_2$, and \mathfrak{G}_3 . The resulting filter functions have undesirable properties that make them poor rational filters.

filter poles and coefficients. Conversely, the red circles indicate the residual levels achieved by the filter obtained by starting SLiSe optimization with the Elliptic filter. The SLiSe filters have significantly lower residual levels than the Gauss and Elliptic filters. Using poles and coefficients from Gauss and Elliptic filters as starting positions for a $q < 10$ results in the same unconstrained SLiSe filter. Although the Gauss and Elliptic are quite different, such result indicates that both of them are in the convex region around the same minimum. The number of iterations in the LM method differs for both starting positions, when starting with the Elliptic filter fewer iterations are required. While we cannot claim optimality for these filters, at least in the unconstrained case, we have never obtained a filter besting the filters obtained by choosing the poles and coefficients of an Elliptic filter as starting positions. In our experience existing filters, and the Elliptic filter in particular, make for excellent starting positions practically eliminating the problem of finding an appropriate starting position.

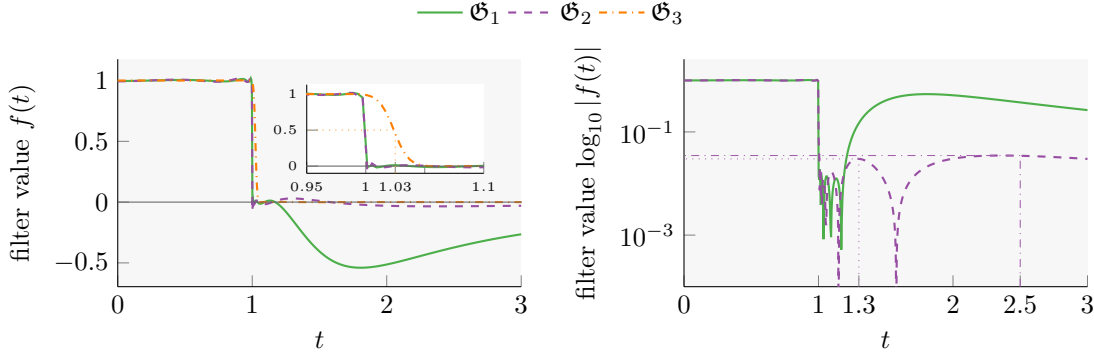
4.4. The Least-Squares Weights $\mathfrak{G}(t)$. The attentive reader might have noticed that we have not yet discussed what causes γ -SLiSe and η -SLiSe from Section 2 to be different filters. Both filters were obtained using the LM optimization method and the Elliptic filter as a starting position. A major difference between the two is the Least-Squares weight function $\mathfrak{G}(t)$ —“weights”, for short—used in the optimization process. As discussed in Remark 3 the optimization process requires some flexibility. The weight function supplies this flexibility, as confirmed by the very different properties of γ -SLiSe and η -SLiSe.

The result of the optimization is invariant under scaling of the weight function so, for the sake of consistency, we consider scaled weight functions with $\mathfrak{G}(0) = 1$. With the flexibility provided by the weight function comes the problem of specifying a weight function that results in a filter with the desired properties. We will see that setting weights without a specific strategy almost certainly yields unexpected results.

We aim for a fire-and-forget approach for the optimization process. In this sense, our target is to obtain the desired results without parameter space exploration. This section contains three guidelines for the choice of the weight functions. The guidelines help the user with the choice of the weights outside the search interval $[-1, 1]$, near its endpoints, and inside it. Each guideline is a heuristic that can be easily implemented as part of an optimization algorithm, or checked manually. These guidelines are an important ingredient for a usable optimization, as following them virtually eliminates the problem of filters with unexpected properties. We provide examples for unexpected properties that occur when violating Guideline 1 and 2. However, if a filter with very specific properties—such as the γ -SLiSe or η -SLiSe filters—is desired, some trial-and-error is unavoidable.

The weight function must be non-zero in an interval larger than just $[-1, 1]$. Otherwise the optimization may result in filters that have large absolute values outside $[-1, 1]$. However, care must be taken when choosing the weights outside the search interval. By tapering the weights too quickly we obtain a steep filter that will nevertheless exhibit insufficient convergence rates. In this context the quality of a filter can be expressed as a function of the filters local extrema outside of the search interval. Specifically, non-increasing local maxima of the absolute function value away from the search interval is a very desirable property. Existing filters already have this property. The Gauss filter, for example, has quickly decaying local extrema.

GUIDELINE 1 (Outside). *Slowly taper off the weights in a large enough neighborhood outside the search interval. In order to avoid trial-and-error, we suggest to detect increasing local maxima*



(a) Linear-scale plot.

Smaller plot: Abscissa limited to $[0.9, 1.1]$.

(b) Semi-log plot.

\mathfrak{G}_3 omitted for better readability.

Fig. 4.3: Plots of filters obtained with three separate weight functions $\mathfrak{G}_1, \mathfrak{G}_2$, and \mathfrak{G}_3 . The resulting functions act as poor rational filters.

of the absolute value of the rational function during the optimization process and increase the weights where required.

By construction, existing filters have a value of 0.5 at the endpoints of the search interval, $f(1) = f(-1) = 0.5$. While not strictly required for most contour solvers, other methods that use rational filters do require a value of 0.5 at the end of the search interval. One example of such a method is the estimation of eigenvalues inside an interval [6]. SLiSe filters are not guaranteed to have a value of 0.5 at the endpoints, unless an appropriate constraint is added to the optimization. In practice SLiSe filters with $f(\pm 1) \approx 0.5$ are easily achievable via appropriate weight functions. Such an approximate value is enough for most applications. By choosing the weight function as symmetric around some region around the endpoint of the search interval we achieve $f(\pm 1) \approx 0.5$. If an exact value is required the filter can be scaled accordingly.

GUIDELINE 2 (Endpoints). *The weight function around the endpoints of the search interval should be chosen symmetrically. Accordingly, during the optimization process, choose $\mathfrak{G}(\pm 1 - \epsilon) = \mathfrak{G}(\pm 1 + \epsilon)$ for $\epsilon \leq 0.2$. Additionally, the optimization procedure should check the weight function for symmetry around the search interval endpoints and, if desired, scale the resulting filter to $f(\pm 1) = 0.5$.*

When the weights inside $[-1, 1]$ are too small the filter function will oscillate inside the search interval. Such oscillations cause the filter value to dip below 1.0, hurting the convergence rate of the entire subspace. We can effectively solve this problem by adjusting the weight function during the optimization process. Previously, we suggested to increase the weights outside the search interval to produce filters with non-increasing local maxima. By the same token we can detect any oscillation inside $[-1, 1]$ and increase the assigned weights accordingly.

GUIDELINE 3 (Inside). *The weights in the entire search interval should be chosen large enough to prevent large oscillations. During the optimization process, monitor the difference between minima and maxima of the filter inside $[-1, 1]$ and adapt weights accordingly.*

Example 1: Very Small Weights Outside the Search Interval. Let us look what happens when the resulting filters were obtained without adhering to one of the three guidelines. In the process of obtaining a replacement candidate for the Elliptical filter the weight function in Table 4.2 could be considered. We will see that \mathfrak{G}_1 and \mathfrak{G}_2 do not correctly taper off the weights outside $[-1, 1]$ and thus violate Guideline 1.

Starting from the assumption that only the weights near the endpoints are relevant, so \mathfrak{G}_1 is chosen with non-zero values only for $|t| < 1.2$. Figure 4.3 shows the filter function obtained with \mathfrak{G}_1 . The filter is a good approximation within $[-1.2, 1.2]$. However, for $|t| > 1.2$, the rational function poorly approximates zero. Such a function would hardly work as a filter. In fact, a value of $f(1.8) \approx -0.5$ for the filter would result in severely degraded convergence rates (see Equation (1.4)). To obtain a better filter it is enough to adjust the weight function to have non-zero values in a

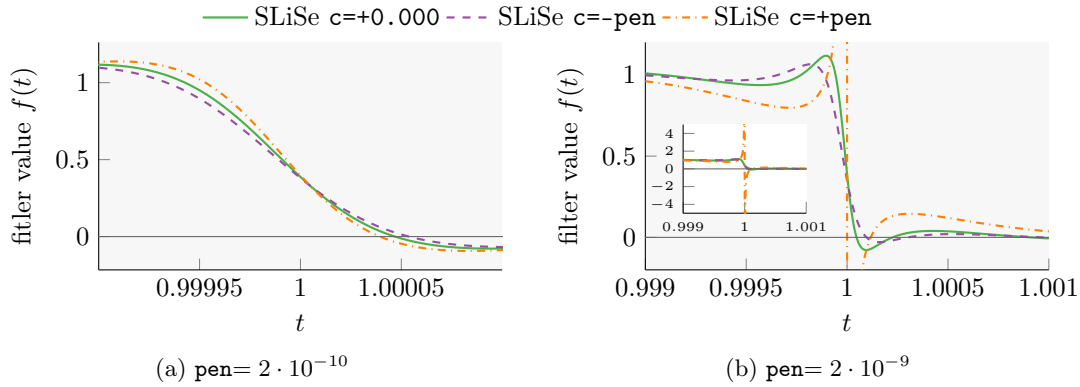


Fig. 4.4: Examples of filters obtained via penalty terms. Left: an appropriately sized penalty parameter yields filters of different steepness. Right: Too large a (positive) penalty parameter results in a pole on the real axis.

larger interval around $[-1, 1]$, for instance $[-5, 5]$. The weight \mathfrak{G}_2 satisfy such a requirement, but the weights taper off very quickly for $t > |1.2|$. The resulting filter function (see Figure 4.3) has values close to zero outside the search interval. Despite this improved behavior, the filter has another more subtle shortcoming. Figure 4.3b shows in a semi-log plot that the filter drops steeply to low values near $[1, 1.2]$, just as desired. However, the filters values inside $[1.2, 3]$ are *larger* than the values inside $[1, 1.2]$. In other words, some of the local maxima outside of the search interval increase away from it, resulting once again in deteriorated convergence rates. Large enough weights in the interval $[1.2 < |t| < 5]$ will result in non-increasing local minima.

Example: Asymmetric Weights Near Endpoints. The weight \mathfrak{G}_3 in Table 4.2 illustrates the results of a weight function that is not symmetric around the endpoint of the search interval, violating the second guideline. In particular, \mathfrak{G}_3 has a larger weight on the inside of the search interval than on the outside. Figure 4.3a plots the resulting filter function as an inlay inside the figure. Assigning a weight of zero between 0.995 and 1.05 results in a filter that fails to drop to zero at the end of the search interval: its value at the endpoint is almost one! Because of the delayed drop the filter crosses the value 0.5 at a later point $f_{\mathfrak{G}_3}(1.025) \approx 0.5$. This behavior does not appear in the filter produced with \mathfrak{G}_1 and \mathfrak{G}_2 as they respect the second guideline: the weights are symmetric around the endpoints $|t| = 1$ and $f(\pm 1) \approx 0.5$ without the need to re-scale the filter. This effect can be understood in terms of the minimization of the squared errors during the function approximation. The continuous drop of the filter function at the endpoints, no matter how steep, incurs in a large squared error. When the weight function lacks symmetry around the endpoint of the search interval, the optimization shifts the drop towards the part of the neighborhood of $[-1, 1]$ with lesser weight. The result is a filter value $f(\pm 1) < 0.5$ if the weight is smaller just inside the search interval, and a value $f(\pm 1) > 0.5$ if the weight is smaller just outside the search interval. Choosing symmetric weights around the endpoints results in $f(\pm 1) \approx 0.5$

4.5. Constrained Optimization. We have seen that the weight function provides some flexibility to the optimization process. However, some desirable properties of a filter cannot be directly influenced by it. In this section we discuss two filter properties that can be achieved by implementing constraints on the optimization. First, we discuss a penalty term on the gradient of the filter function, which results in filters of varying 'steepness' and with varying amounts of 'overshooting'. Given our standard search interval, $[-1, 1]$, we call the derivative of the filter $f(t)$ at the endpoints of the interval $\nabla_t f(t)|_{t=1} = -\nabla_t f(t)|_{t=-1}$ the *steepness* of the filter. The steepness—or separation factor—of a filter has previously been suggested as a quality measure in the context of optimizing exclusively the coefficients of the rational function [26]. A steep filter is considered desirable because it dampens eigenvalues outside the search interval even when the eigenvalues are close to the interval endpoints and, in doing so, improves convergence. When optimizing the poles of the rational functions together with its coefficients the steepness alone does not serve as

c	Residual	Steepness
0	2.265829×10^{-5}	-1.211081×10^4
-2×10^{-10}	2.279018×10^{-5}	-1.063877×10^4
$+2 \times 10^{-10}$	2.288353×10^{-5}	-1.429542×10^4

Table 4.3: Residual levels and steepness of the filter functions shown in Figure 4.4a.

a good measure of quality anymore. It is possible for a filter to be steep, and yet not to dampen eigenvalues outside of the search interval sufficiently well. The lack of dampening is due to an effect called “overshooting”, corresponding to a filter that greatly exceeds its target value. Overshooting is a known behavior when approximating discontinuous functions with continuous ones. Usually a very steep filter tends to overshoot at the endpoint of $[-11]$, and conversely filters that do not overshoot are not particularly steep.

In Section 4.5.1 we discuss how to adjust the optimization to generate filters of varying steepness, and thus also with varying amounts of overshooting. A *penalty term* can modify the optimization procedure to influence the steepness. By adding a term to the residual level function we penalize filters that are not desirable by a factor of c , the penalty parameter.

$$\min_{w_i, \gamma_i} \left[\|h - f(w, \gamma)\|_2^2 + \frac{c}{2} \cdot [\nabla_t f(t)|_{t=1} - \nabla_t f(t)|_{t=-1}] \right]. \quad (4.9)$$

Note that since $\nabla_t f(1)$ is supposed to be negative, a positive c will make for a steeper filter when minimizing the residual. Solving the optimization problem requires straight-forward changes to the gradient.

Section 4.5.2 describes a different kind of constraint, namely box constraints on the imaginary part of the poles. Such a constraint may be advantageous when Krylov solvers are used for the linear system solves as they appear in Equation (1.2). The condition number of the shifted matrix $A - w_i I$ may become large when $|\Im m(w_i)|$ is small, which can occur for large degrees of the Elliptic and SLiSe filters. One possible way to circumvent this problem is to ensure that the absolute value of the imaginary part for each pole is large enough. For SLiSe filters this translates into a box constraint d on the parameters:

$$\min_{w_i, \gamma_i} \left[\|h(t) - f(t, w, \gamma)\|_2^2 \quad \text{s.t.} \quad \forall i : |\Im m\{w_i\}| \geq d \right] \quad (4.10)$$

Both constrained optimization approaches presented in this section are not fire-and-forget; some trial and error is always required for the parameter selection. This lack of robustness for the parameter selection is the exception in our work. Constrained optimization without the need for extensive parameter selection is an area of future work.

4.5.1. Steepness and Overshooting via Penalty Term. Before we look at some examples of filters obtained with penalty terms, let us consider how the steepness and overshooting influence the convergence behavior of the filter by comparing γ -SLiSe and the Gauss filter from Figure 2.2a. By starting to drop significantly earlier than the endpoint of the search interval at $t = 1$, the Gauss filter is significantly less steep than the SLiSe filter. Conversely, the SLiSe filter maintains a value close to one inside the search interval closer to the endpoint, and it takes small values just outside the search interval. The increased steepness of the γ -SLiSe filter comes at the cost of overshooting. Figure 2.2a clearly shows that the SLiSe filter shoot up above 1 and drops below 0 just inside and outside the search interval respectively. In terms of the convergence rate, the surge above 1 is not a problem, however the overshooting outside $[-11]$ is an undesirable effect. An overshooting filter maps eigenvalues to relatively large negative—and thus large in magnitude—values outside the endpoints, hurting convergence.

While it is possible to increase the steepness of SLiSe filters via the penalty term, there is little benefit in even steeper filters with more overshooting. Figure 4.4a shows an illustrative

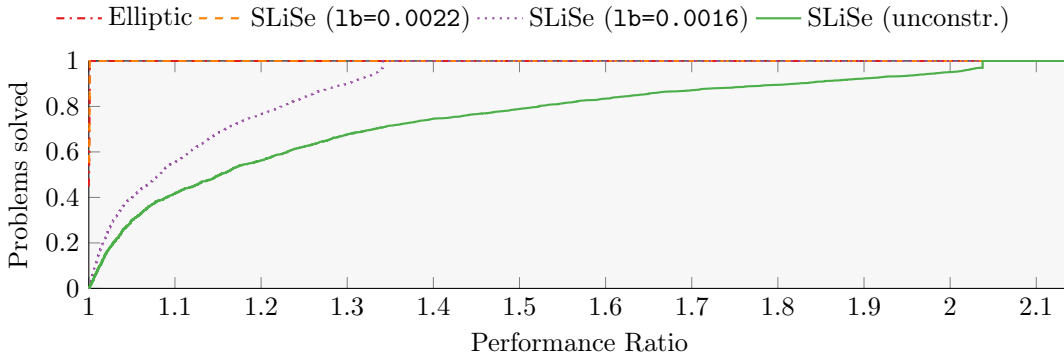


Fig. 4.5: Performance profile comparing the worst condition number for the linear systems arising from filter application to 2116 problems obtained from the “Si2” matrix. The performance ratio for the Elliptic and SLiSe (1b=0.0022) filters are one over the entire abscissa range.

example of filters obtained with an appropriately sized penalty parameter and number of poles per quadrant $q = 4$. Table 4.3 shows the residuals without penalty term and the steepness of the filter $\nabla_t f(1)$ for the resulting filters. The figure makes plain how a negative penalty term tends to decrease steepness and overshooting while a positive c increases them. Since the penalty parameter is chosen significantly smaller than the residual, the change to the filter is not very pronounced. Choosing the penalty parameter to be larger is not without hazards, especially when c is chosen to be positive. Figure 4.4b shows a filter generated with a larger value for c , again with $q = 4$. Such a filter has a pole on the real axis which results in a very steep slope, but not an effective filter. For one thing, the pole causes significant overshooting which substantially hurts convergence. Additionally, a real pole affects the corresponding linear system, which can become seriously ill-conditioned causing failure or slow converge of the iterative solver. While a large and positive parameter is problematic because of the risk of a real pole, this is usually not a concern in practical applications. Often, it is more important to limit the overshooting than it is to make the already steep SLiSe filters even steeper. Figure 4.4b shows that a negative penalty parameter c reduces overshooting⁶. η -SLiSe was obtained using a negative penalty parameter, which we discuss further in Section 4.6.

4.5.2. Large Imaginary Parts via Box Constraints. Implementing box constraints in our framework is straightforward: Instead of the old update step in Equation (4.2) we use gradient projection by updating as follows

$$x^{(k+1)} = \mathcal{P}(x^{(k)} - s \cdot \nabla_x F(x)|_{x=x^{(k)}}), \quad s \geq 0, \quad (4.11)$$

where $\mathcal{P}(x)$ projects x into the constraints. In practice we project onto the constrained value whenever the constraint is violated. We implement this scheme by forcing the absolute value of the imaginary part of every pole to be equal or larger than some value $1b$. For a single pole w_l the projection would be

$$\mathcal{P}(w_l) = \begin{cases} \Re(w_l) + i \cdot \text{sgn}(\Im(w_l)) \cdot 1b & |\Im(w_l)| < 1b \\ \Re(w_l) + i \cdot \Im(w_l) & \text{otherwise} \end{cases}$$

In the following, we compare filters with different box constraints. Figure 4.5 shows four filters each with $q = 4$. Shown are the Elliptic filter, a SLiSe filter obtained via unconstrained optimization⁷, and two additional SLiSe filters obtained with different $1b$ constraints. For the Elliptic filter $\min_{1 \leq i \leq q} |\Im(w_i)|$ is about 0.0022, while it is 0.001 for the unconstrained SLiSe filter. In the case of the constrained SLiSe filters, we consider “SLiSe (1b=0.0022)” filter, with

⁶Some trial and error may be required to obtain a penalty parameter of appropriate size.

⁷The weights are available in Appendix C under “Box-SLiSe”.

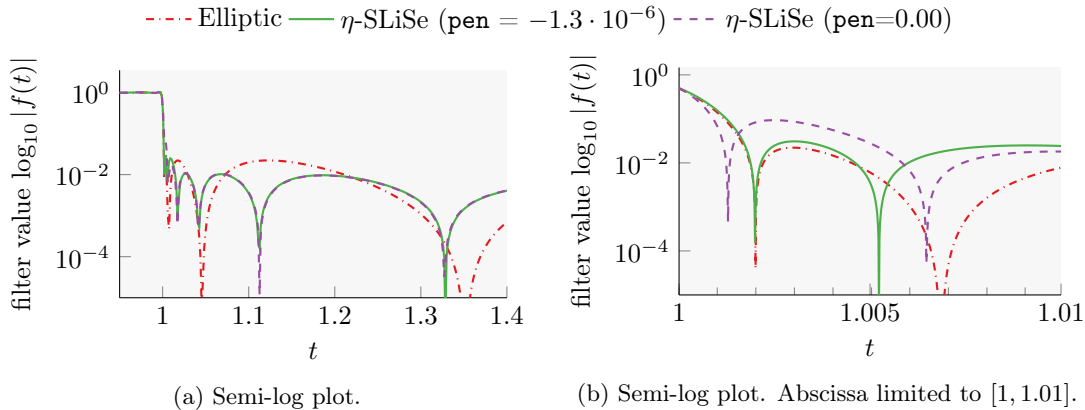


Fig. 4.6: Plots of the Elliptic filter, η -SLiSe, and the η -SLiSe filter without penalty term. All filters have 16 poles and coefficients.

a $1b$ corresponding to the Elliptic filter. Additionally, we also examine “SLiSe ($1b=0.0016$)” generated with a constraint of 0.0016, about half a way between the Elliptic and the unconstrained filter. We calculate the condition number for each of the shifted linear systems that result from filter application on the 2116 problems extracted from the “Si2” matrix as illustrated in Section 2. Figure 4.5 is a performance profile of the largest condition number for each of the benchmark problems. The Elliptic filter and the SLiSe ($1b=0.0022$) perform identically in the performance profile. Both filters have a value of one over the entire abscissa range, which indicates that the condition numbers are the same. The figure implies that the largest condition number is influenced solely by the smallest absolute imaginary value of the poles. Accordingly, the constrained filter with $1b$ of 0.0016 performs worse, and the unconstrained SLiSe filter is the worst. This effect can be understood by realizing that the shifted matrices $A - Iw_l$ become nearly singular only if w_l is near an eigenvalue of A .

An increase in the $1b$ constraint has a large influence on the filter. As a result, caution is required when optimizing with box constraints. For example, for a choice of weight function that follow Guideline 1 from Section 4.4 in the unconstrained case, the same is not necessarily true when optimizing a filter with box constraints. We discuss an example filter with box constraints in the next section.

4.6. A Rich Variety of Filters: Practices and Experience. In the previous sections we have discussed a number of techniques to influence the optimization procedure. Now we are going to illustrate three filters that highlight the potential of these optimization parameters. First, we discuss η -SLiSe, where a penalty parameter is used to limit overshooting. Second, we present a filter that violates Guideline 1 from Section 4.4 and yet exhibits good rates of convergence on our set of benchmark problems. Third, we present a filter that uses box constraints to achieve better condition numbers for the shifted matrices that arise from the filter application. Despite the Gauss filter is the one most often used in real-world applications, in this section we put a strong emphasis on alternatives for the Elliptic filter. The Elliptic filter is an interesting case study, because its rate of convergence is worst-case optimal. We focus on improving over the Elliptic filter to illustrate the power of SLiSe filters.

Penalty parameter: η -SLiSe. We have seen η -SLiSe in Section 2.2, where we compare its convergence rate to the Elliptic and Gauss filters. η -SLiSe was obtained via a negative penalty parameter, to limit the overshooting of the filter. Without the penalty term the filter would perform significantly worse.

Figure 4.6 shows the Elliptic and η -SLiSe filter. Additionally, we include the unconstrained version of η -SLiSe, being the filter obtained with the same weights as η -SLiSe but without penalty term. Figure 4.6a shows an abscissa range of $[0.95, 1.4]$. At this scale both SLiSe filters look identical. Both filters oscillate less than the Elliptic filter, which we would expect from the rate of

convergence for η -SLiSe. Figure 4.6b shows the same filters for an abscissa range of $[1, 1.01]$, just outside the search interval. At this scale, the two SLiSe filters are very different. The SLiSe filter without penalty term is steeper and overshoots more than the Elliptic filter, which results in larger absolute function values inside $[1.001, 1.006]$. The penalty parameter for η -SLiSe was chosen large enough to make the filter about as steep as the Elliptic filter. As a result, η -SLiSe overshoots less than the unconstrained filter and oscillates at a magnitude only slightly larger than the Elliptic filter. Compared to the Elliptic filter, η -SLiSe trades-off a slightly larger (absolute) function values near the end of the search interval for much smaller values farther away.

In this example, the penalty parameter is chosen to be of large absolute value, as compared to the values in Section 4.5.1. Such a large penalty parameter results in a significant reduction in the steepness and overshooting of the filter. The difference between the SLiSe filters with and without penalty term is large near the end of the search interval, but negligible in $[1.05, \infty]$. The “design procedure” for such a filter is straight forward: first, we chose the weights such that the filter has the desired behavior for most of the t axis, e.g., $[0, 1] \cup [1.05, \infty]$ and such that the filter overshoots slightly more than desired. Then, we used a negative penalty term to lessen the overshooting; this step usually requires only very few iterations and so can be done very quickly.

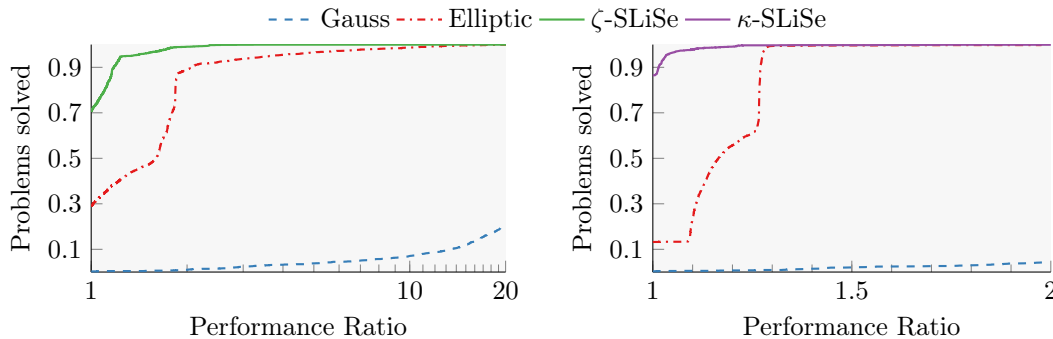
Breaking Guideline 1: ζ -SLiSe. We specifically advocate 3 guidelines for the choice of weight function in Section 4.4. However, when done judiciously breaking these guidelines can be advantageous, as we illustrate in this section. We discuss ζ -SLiSe a filter that violates Guideline 1; this filter also aims to replace the Elliptic filter.

Figure 4.7a shows a performance profile of the Gauss, Elliptic, and ζ -SLiSe filter that compares the rates of convergence for these filters. The setup is the same as in Section 2.2: we use the same 2116 intervals taken from the “Si2” matrix, $\mathbf{p} = \mathbf{m}$, and all filters have 16 poles. The Gauss filter performs similar to the performance profile in Section 4.4. ζ -SLiSe filter not only performs better than the Elliptic filter, it appears to perform better than η -SLiSe! η -SLiSe achieves a better rate of convergence than the Elliptic filter for only 50% of the problems, whereas ζ -SLiSe does so for 70% of the problems. The performance profile also encodes a more subtle difference: In Figure 4.7a $f_{\text{Elliptic}}(2.35) \approx 0.92$, which indicates that ζ -SLiSe exhibits rates of convergence better than 2.35 times the rate of the Elliptic filter for 8% of the benchmark problems. This is not the case for η -SLiSe, where $f_{\text{Elliptic}}(2.35) \approx 0.999$.

It appears that ζ -SLiSe would be a better replacement for the Elliptic filter. However, the filter does not conform to Guideline 1. The filter has a single local extremum that has a significantly larger absolute value than both of its neighboring extrema. This extremum is still smaller than the equi-oscillation of the Elliptic filter, which is the reason the why ζ -SLiSe performs better than the Elliptic filter. The 8% of benchmark problems where ζ -SLiSe performs significantly better than the Elliptic filter are exactly those where no eigenvalue coincides with this larger local extremum of ζ -SLiSe. It is possible to obtain filters that violate our guidelines and still yield good convergence rates, as illustrated by ζ -SLiSe. However, adhering to our guidelines vastly simplifies the creation of filters. For that reason, we propose η -SLiSe, and not ζ -SLiSe, as a replacement for the Elliptic filter.

Box Constraint: κ -SLiSe. There is another problem with ζ -SLiSe. The filter has a pole with an absolute imaginary value of $\min_{1 \leq i \leq q} |\Im m(w_i)| \approx 0.001$. Analogously to the filters discussed in Section 4.5.2 this deteriorates the convergence of Krylov-based linear system solvers. To mitigate this problem we can use box constraints to obtain a filter where each pole has an absolute imaginary value of at least 0.0022, the corresponding value for the Elliptic filter. We discuss a filter called κ -SLiSe, obtained with a box constraint of $\mathbf{1b} = 0.0022$ and the same weight function used to obtain ζ -SLiSe. κ -SLiSe violates Guideline 1, just as ζ -SLiSe does.

Figure 4.7b shows the performance profile for κ -SLiSe. The box constraint results in two changes of κ -SLiSe as compared to the ζ -SLiSe. First, the box constraint contribute to lessen the overshooting of the filter. As a result κ -SLiSe attains a better rate of convergence than the Elliptic filter for 86% of the benchmark problems, as compared to the 70% of ζ -SLiSe. Second, κ -SLiSe has larger (as compared to ζ -SLiSe) absolute function values for most of the t axis, which results in rates of convergence that are closer to the rates of the Elliptic filter. The larger absolute function values cause Figure 4.7b to look roughly like a version of Figure 4.7a compressed along the abscissa.



(a) The same performance profile zoomed into [1, 20] (b) The same performance profile zoomed into the interval [1, 2].

Fig. 4.7: Semi-log performance profile of the convergence rate for the Gauss, ζ -SLiSe, and Elliptic filters. All filters have 16 poles and $\mathbf{p} = \mathbf{m}$. Both filters violate Guideline 1.

From the performance profile we can infer that the convergence rates of κ -SLiSe are only slightly better than those of the Elliptic filter.

Section 4.5.2 already illustrates that box constraints can effectively decrease the condition number of the linear systems that arise in the application of the filter. The condition numbers of the linear systems for κ - and ζ -SLiSe are very similar to the ones shown in Figure 4.5. κ -SLiSe illustrates that box constraints can be used to obtain SLiSe filters with good convergence rates. Nevertheless, larger box constraints usually tend to result in worse rates of convergence, as compared to an unconstrained filter. While κ -SLiSe is still marginally better than the Elliptic filter, it yields rates of convergence that are not nearly as good as ζ -SLiSe or η -SLiSe.

5. Related Work. Contour based eigensolvers can be described as a family of methods based on Cauchy’s Residue Theorem. The name “contour based” stems from an integration of the matrix resolvent along a contour. These contour integrals are calculated via numerical quadrature which inevitably results in linear system solves and reduced eigenvalue problems through a Rayleigh-Ritz projection. Recently these methods have gained popularity when used to solve the interior eigenvalue problem. This popularity is in part due to the eigensolver’s support for non-Hermitian and generalized eigenproblems, and to an additional level of parallelism compared to traditional iterative methods. One important aspect of contour methods is that they typically tend to avoid operations on long vectors, e.g, re-orthogonalization.

Two well-known contour based eigensolvers are the SS family of solvers due to Sakurai and Sugiura [24], and FEAST due to Polizzi [22]. Early work by Sakurai and Sugiura on contour based solvers resulted in the SS-Hankel method, a non-iterative method based on complex moment matrices. A different approach is taken by Polizzi’s FEAST, which is an iterative contour based solver. Underlying FEAST is a Rayleigh-Ritz procedure where the contour integral is used to improve convergence. Later work by Sakurai et. al. resulted in a Rayleigh-Ritz type method [9, 10] and various block methods [12]. Beyn proposed a similar method in [3]. Despite the rich variety of recent works, contour based solvers are still a very active area of research where most of the focus is on improving the performance and robustness of the algorithms and their implementations. A recent comparison of common contour based solvers is available in [11].

A key insight to the use of numerical quadrature for the contour integration is the correspondence between contour methods and rational matrix functions: one can reinterpret the numerical quadrature of the matrix resolvent $(A - zI)^{-1}$ as a rational filter. From this point of view contour methods can be considered as part of the richer mathematical field of rational function approximation. The correspondence between contour methods and rational filters was discussed for FEAST in [25], for SS-H in [10], and for SS-R in [9]. Early on Murakami proposed the use of classic rational filters from signal processing [17–21] in the “filter diagonalization method”; for a discussion of this work we refer to [1]. For FEAST the Elliptical filters were proposed in [8] to improve

load balancing and (in some cases) convergence behavior. The rational function point-of-view also enables the development of specialized algorithms: for instance, for real-symmetric matrices it is possible to avoid complex-arithmetic entirely [1].

More recently the filter itself has been treated as a parameter that can be designed via optimization methods. Van Barel [2] proposed a non-linear Least-Squares approach for non-Hermitian filters within the SS-H framework, while Xi and Saad [26] described linear Least-Squares optimized filters for the Hermitian FEAST solver. Since Van Barel’s approach is geared towards non-Hermitian eigenproblems, it is not possible to make use of the conjugate or reflection symmetry. The resulting degrees of freedom make for a more difficult optimization problem. By requiring a parameter space search, his approach results in filters that are not as robust as our SLiSe. Van Barel’s Least-Squares optimization is based on the discrete ℓ_2 norm, not a function approximation approach. Even in the case of Hermitian problems, optimizing the squared distances in only a sample of points must be done with great care. Choosing too small a number of sample points can have undesirable effects: it is possible to obtain poles near the real axis which are not detected by the sample points. On the other hand having a large number of sample points is very expensive. Finally, Van Barel’s approach does not support constraints, as we present in Section 4.5.

A FEAST related approach for linear Least-Squares optimized filters [26] focuses on the Hermitian eigenproblem. In this work, not the poles but only the coefficients of the rational function are optimized. The result is a robust process that is much easier to solve, at the cost of being less expressive. An optimization approach that does not optimize poles is limited by the initial choice of them. As we have shown in this work, the process of optimizing a SLiSe filter significantly moves the poles inside the complex plane. On the opposite, fixing the poles imposes a constraint on the optimization that is even larger than constraining just their imaginary part as illustrated in Section 4.6. In practice, when optimizing solely the coefficients of the rational approximation, the optimization algorithm behaves very differently. For example, positive penalty parameters work much better in Xi and Saad’s approach, because real poles cannot occur.

6. Conclusions. In this work we illustrate how a weighted non-linear Least-Squares optimization of rational filters provides a rich framework of solutions that can be employed in contour based eigensolvers. In our approach we optimize both the pole placement and the coefficients of the rational filters, which leads to a non-convex problem. Because of its non-convexity the solution of such problem has to be approached with care. First we stabilize the optimization process by explicitly formulating the filters to be conjugation and parity invariant. In addition to stabilizing the target function, such symmetries reduce the complexity of the optimization process by a factor up to four. Due to the non-convexity of the problem, convergence to an optimal solution is not easily guaranteed. We show that a careful selection of the starting position and an appropriate optimization algorithm, e.g. the Levenberg-Marquardt method, lead to solutions with systematically smaller residuals as the degree of the filter is increased.

We show that using our optimized rational SLiSe filters can significantly improve the efficiency of contour based eigensolvers on a given problem. In particular we show that an optimized filter can improve the convergence of the subspace iteration for a large set of cases. In the specific instances of the standard Gauss and Elliptic filters we show-case the flexibility of our approach by providing SLiSe replacements. This flexibility is achieved via a skillful selection of Least-Squares weights and by the use of constrained optimization. We illustrate that optimization with box constraints can also usefully address the issue of rational filters with poles very close to the real axis, which lead to almost singular matrix resolvents. Such constrained optimization decreases the condition number of the resolvents, which positively influences the solution of the corresponding linear system solves when Krylov based methods are employed.

Significant effort went into the usability of the optimization process. The entire approach is designed to be fire-and-forget, without requiring many optimization processes for parameter space exploration. While we largely succeeded in our aim, there are still corner cases where some parameter space exploration is required to obtain usable filters. For instance, some trial-and-error is required for constrained optimization. More robust optimization approaches, especially for constraints, is a topic for future work. The ultimate goal is to provide filters that adapt to a given specific problem. Such filters would be generated on-the-fly and take advantage of spectral

information, if cheaply available. Not only do problem-specific filters promise better convergence, but they can provide automatic load balancing between multiple contour ‘‘slices’’. The present work is meant as a significant step towards such a direction.

Acknowledgments. Financial support from the Jülich Aachen Research Alliance High Performance Computing and the Deutsche Forschungsgemeinschaft (DFG) through grant GSC 111 is gratefully acknowledged.

Appendix.

A. Definite integrals. For the convenience of the reader, we provide the definite integrals required to compute the residual level function $F(\gamma, \omega)$ from Equation (3.15), the gradient ∇F from Equations (3.19) and (3.19), and the approximation of the Hessian, given in Equation (4.8). For the sake of generality we denote poles as ω_1 and ω_2 , without conjugation although some formulation require the conjugation or sign change of ω_1 or ω_2 . Recall that the functions $\mathfrak{G}(t)$ and $h(t)$ are piecewise constant and determine the integral boundaries, written as a and b .

The calculation of $W_{k,\ell}$, $\overline{W}_{k,\ell}^\pi$, $X_{k,\ell}$, $\overline{X}_{k,\ell}^\pi$, $Y_{k,\ell}$, and $Z_{k,\ell}$ requires the following integral:

$$\int_a^b \frac{dt}{(t - \omega_1)(t - \omega_2)} = \frac{1}{\omega_1 - \omega_2} \left[\ln \frac{(b - \omega_1)}{(a - \omega_1)} + \ln \frac{(a - \omega_2)}{(b - \omega_2)} \right]$$

For the ‘diagonal’ terms $W_{k,k}$ and $\overline{X}_{k,k}^\pi$ it holds that $\omega_1 = \omega_2$. In this case we can re-write the expression without logarithms. This integral is also required for $\overline{\nabla \theta}_k$:

$$\int_a^b \frac{dt}{(t - \omega_1)^2} = \frac{b - a}{(b - \omega_1)(a - \omega_1)}$$

Note that this is not the case for the X , Z , and Y , where the signs and/or conjugations of ω_1 and ω_2 differ.

For θ_k and $\overline{\theta}_k^\pi$ we require the following integral:

$$\int_a^b \frac{dt}{t - \omega_1} = \ln \frac{(b - \omega_1)}{(a - \omega_1)}$$

The calculation of $\overline{\nabla W}_{k,\ell}$, $\nabla X_{k,\ell}$, $\overline{\nabla Y}_{k,\ell}$, and $\nabla Z_{k,\ell}$ requires the integral:

$$\int_a^b \frac{dt}{(t - \omega_1)^2(t - \omega_2)} = \frac{b - a}{(\omega_1 - \omega_2)(b - \omega_1)(a - \omega_1)} - \frac{\ln \frac{(b - \omega_1)}{(a - \omega_1)}}{(\omega_1 - \omega_2)^2} + \frac{\ln \frac{(b - \omega_2)}{(a - \omega_2)}}{(\omega_1 - \omega_2)^2}$$

The ‘diagonal’ term $\overline{\nabla W}_{k,k}$ can again be expressed without logarithm:

$$\int_a^b \frac{dt}{(t - \omega_1)^3} = (b - a) \left[\frac{b + a - 2\omega_1}{(b - \omega_1)^2(a - \omega_1)^2} \right]$$

In the approximation of the Hessian the terms $\nabla \overline{\nabla W}_{i,j}$, $\overline{\nabla \nabla X}_{i,j}$, $\nabla \overline{\nabla Y}_{i,j}$, and $\overline{\nabla \nabla Z}_{i,j}$ require yet another integral. This one is given by:

$$\begin{aligned} \int_a^b \frac{dt}{(t - \omega_1)^2(t - \omega_2)^2} &= \frac{a - b}{(\omega_1 - \omega_2)^2} \left[\frac{1}{(a - \omega_1)(-b + \omega_1)} + \frac{1}{(a - \omega_2)(-b + \omega_2)} \right] \\ &+ \frac{2}{(\omega_1 - \omega_2)^3} \left[\ln \frac{a - \omega_1}{b - \omega_1} + \ln \frac{b - \omega_2}{a - \omega_2} \right] \end{aligned}$$

Here the ‘diagonal’ term is given by:

$$\int_a^b \frac{dt}{(t - \omega_1)^4} = \frac{1}{3} \left[\frac{1}{(a - \omega_1)^3} + \frac{1}{(-b + \omega_1)^3} \right]$$

B. Obtaining benchmark problems from a matrix. In this short appendix we discuss a method to generate a large set of intervals \mathcal{I} from a given eigenproblem corresponding to an Hermitian matrix A . The objective is to obtain a benchmark test set for filtered subspace iteration, as a means to compare filters without having to solve each problem separately.

Interior eigensolvers based on filtered subspace iteration are sensitive to the spectrum of A near the search interval \mathcal{I} . Thus, the choice of the search intervals is critical for testing an interior eigensolver. Users often select the search interval motivated by some structure in the spectrum of A , such as the HOMO-LUMO gap in Density Functional Theory methods. Our aim is to create a large set of intervals that represent a variety of real-world use-cases, especially those based on the selection of intervals influenced by the structure of the spectrum. To this end, we propose a method to obtain search intervals by exploiting the distribution of the eigenvalues of A . Instead of choosing the intervals directly, we compute a set of endpoints $E = \{a_1, a_2, \dots\}$, and then form intervals $\mathcal{I}_{i,j} = [a_i, a_j]$ with $a_i, a_j \in E$ and $a_i < a_j$.

These endpoints should represent the neighborhood of an identifiable spectral feature, such as a spectral gap or a cluster; we refer to them as “feature points”. Given a function $\phi \in C^2$ that approximates the eigenvalue density, we consider feature points to be the real zeros of the first and second derivative of ϕ . A good candidate for ϕ can be obtained, for example, via the Kernel Polynomial Method (KPM) which constructs a polynomial of degree M that approximates the spectral density. The zeros of ϕ' are stationary points; assuming that ϕ is a good approximation of the eigenvalue density, a local maximum may indicate a high density of eigenvalues or even a cluster. corresponds to a potential gap in the spectrum. Inflection points of ϕ may indicate a change in the increase or decrease of the (approximated) eigenvalue density, signaling a relatively small spectral gap. By choosing a large $M \approx 45$ it is possible to obtain thousands of intervals for a single matrix A . The large problem set can be used to obtain the subspace convergence rates and the condition numbers of the linear system solves without solving each eigenproblem in the benchmark set. Such an approach is limited by the availability of the entire spectrum of A , and thus is only applicable for small to medium sized eigenproblems.

For instance, the subspace convergence rate (see Equation (1.4)) depends only on the filter value for the eigenvalues. If the entire spectrum of A is available, we can obtain the convergence rate by computing these values directly. In the same fashion, each filtered interval results in a number of shifted linear system solves of the form $A - Iz_i$ (see Equation (1.1)). When Krylov-based methods are used to solve these systems, the overall performance depends on the condition number. Since A is Hermitian, the shifted matrix is still normal. As a result the singular values of $A - Iz_i$ are given by $\sigma_i = |\lambda_i - z_i|$, where λ_i is the i^{th} eigenvalue of A . By proceeding in this manner for all the poles z_i , we can inexpensively obtain the condition number for all the system solves. Usually, the solve with the highest condition number dictates the overall performance, which is what we used to motivate our analysis of box constraints in Section 4.5.2.

C. List of filters. The filters presented in Section 2 are provided here. For a given filter function

$$f(t, w, \gamma) = \sum_{k=1}^q \left[\frac{\gamma_k}{t - w_k} + \frac{\bar{\gamma}_k}{t - \bar{w}_k} - \frac{\gamma_k}{t + w_k} - \frac{\bar{\gamma}_k}{t + \bar{w}_k} \right]$$

we provide only the poles in the "first quadrant" of the complex plane—that is, the poles with positive real and imaginary parts—and the corresponding coefficients γ .

$ t \in$	[0, .95)	[.95, 1.05)	[1.05, 1.4)	[1.4, 5)	[5, ∞)
$\mathfrak{G}_{\gamma\text{-SLiSe}}(t)$	1	.01	10	20	0
$ t \in$	[0, .95)	[.95, .995)	[.995, 1.005)	[1.005, 1.05)	[1.05, 1.1)
$\mathfrak{G}_{\eta\text{-SLiSe}}(t)$	1	4	0.5	4	0.6
$\mathfrak{G}_{\text{Box-SLiSe}}(t)$	1	4	2	4	0.6

$ t \in$	[1.1, 1.3)	[1.3, 1.8)	[1.8, 3)	[3, ∞)
$\mathfrak{G}_{\eta\text{-SLiSe}}(t)$ (cont'd)	1	0.3	0.1	0
$\mathfrak{G}_{\text{Box-SLiSe}}(t)$ (cont'd)	1	0.3	0.1	0

Table C.1: Weight functions for filters discussed in this paper.

Poles ω	Coefficients γ
$0.999687712591797 + 0.0117367635577924i$	$0.006050012497458 - 0.000227036554136i$
$0.991596517222374 + 0.093208856178882i$	$0.021484299350510 - 0.003666847993474i$
$0.903848148311606 + 0.327740045699974i$	$0.055938387061383 - 0.032384567818443i$
$0.440319857798568 + 0.732970137475905i$	$0.054079510922005 - 0.122837701171251i$

Table C.2: $\gamma\text{-SLiSe}$, a filter meant to replace the Gauss filter

Poles ω	Coefficients γ
$0.999986323489133 + 0.002453510792541i$	$0.00110213725846833 - 7.98515806042 \cdot 10^{-6}i$
$0.999401600189637 + 0.024159213959740i$	$0.00768847889630669 - 0.000333793441122i$
$0.983469964312691 + 0.160816338804574i$	$0.04592568742949140 - 0.00885856519222i$
$0.628559997051189 + 0.718255201795431i$	$0.11139119375850727 - 0.147357486573937i$

Table C.3: $\eta\text{-SLiSe}$, a filter meant to replace the Elliptic filter. Obtained with a penalty parameter of $c = -1.3 \cdot 10^{-6}$

Poles ω	Coefficients γ
$0.999517437449349 + 0.0011346403206723i$	$0.000600799688893 - 0.0001380523176106i$
$0.996122208058289 + 0.0169588203859498i$	$0.006148402177611 - 0.0012349951550185i$
$0.971590779276380 + 0.1314326323772290i$	$0.039288214664051 - 0.0095779819369782i$
$0.632009932807876 + 0.6589465004506030i$	$0.111997418650841 - 0.1454789177402232i$

Table C.4: $\zeta\text{-SLiSe}$, a filter meant to replace the Elliptic filter that violates Guideline 1

Poles ω	Coefficients γ
$0.999997864241235 + 0.002199301304944i$	$0.000920693720425 - 2.62225614322 \cdot 10^{-6}i$
$0.999817083735386 + 0.019255687759249i$	$0.006309876577596 - 0.000106451402529i$
$0.993359173161426 + 0.135785991680408i$	$0.040771709455088 - 0.003927802442013i$
$0.694622923894908 + 0.732441949783473i$	$0.135841041422952 - 0.150283641573960i$

Table C.5: $\kappa\text{-SLiSe}$, a filter meant to replace the Elliptic filter with Krylov solvers that violates Guideline 1. Obtained with a box constraint of $\mathbf{1b} = 0.0022$

REFERENCES

- [1] A. P. AUSTIN AND L. N. TREFETHEN, *Computing Eigenvalues of Real Symmetric Matrices with Rational Filters in Real Arithmetic*, SIAM J. Sci. Comput., 37 (2015), pp. A1365–A1387.
- [2] M. V. BAREL, *Designing Rational Filter Functions for Solving Eigenvalue Problems by Contour Integration*, Linear Algebra Appl., 502 (2016), pp. 346 – 365.
- [3] W.-J. BEYN, *An Integral Method for Solving Nonlinear Eigenvalue Problems*, Linear Algebra and Its Applications, 436 (2012), pp. 3839–3863.
- [4] S. BOYD AND L. VANDENBERGHE, *Convex Optimization*, Cambridge University Press, 2004.
- [5] T. A. DAVIS AND Y. HU, *The University of Florida Sparse Matrix Collection*, ACM Trans. Math. Softw., 38 (2011), pp. 1:1–1:25.

- [6] E. DI NAPOLI, E. POLIZZI, AND Y. SAAD, *Efficient Estimation of Eigenvalue Counts in an Interval*, Numer. Linear Algebra Appl., 23 (2016), pp. 674–692.
- [7] E. D. DOLAN AND J. J. MORÉ, *Benchmarking Optimization Software With Performance Profiles*, Mathematical Programming, 91 (2002), pp. 201–213.
- [8] S. GÜTTEL, E. POLIZZI, P. T. P. TANG, AND G. VIAUD, *Zolotarev Quadrature Rules and Load Balancing for the FEAST Eigensolver*, SIAM J. Sci. Comput., 37 (2015), pp. A2100–A2122.
- [9] T. IKEGAMI AND T. SAKURAI, *Contour Integral Eigensolver for non-Hermitian Systems: A Rayleigh-Ritz-type Approach*, Taiwanese J. Math., 14 (2010), pp. pp–825.
- [10] T. IKEGAMI, T. SAKURAI, AND U. NAGASHIMA, *A Filter Diagonalization for Generalized Eigenvalue Problems Based on the Skaurai-Sugiura Projection Method*, J. Comput. Appl. Math., 233 (2010), pp. 1927 – 1936.
- [11] A. IMAKURA, L. DU, AND T. SAKURAI, *Relationships Among Contour Integral-Based Methods for Solving Generalized Eigenvalue Problems*, Japan J. Indust. Appl. Math, 33 (2016), pp. 721–750.
- [12] A. IMAKURA AND T. SAKURAI, *Block Krylov-type Complex Moment-based Eigensolvers for Solving Generalized Eigenvalue Problems*, Numerical Algorithms, (2016), pp. 1–21.
- [13] V. KALANTZIS, J. KESTYN, E. POLIZZI, AND Y. SAAD, *Domain Decomposition Approaches for Accelerating Contour Integration Eigenvalue Solvers for Symmetric Eigenvalue Problems*. Preprint submitted to SISC.
- [14] K. LEVENBERG, *A Method for the Solution of Certain Non-Linear Problems in Least Squares*, Q. Appl. Math., 2 (1944), pp. 164–168.
- [15] K. MADSEN, H. B. NIELSEN, AND O. TINGLEFF, *Methods for Non-Linear Least Squares Problems*, tech. report, Technical University of Denmark, 2004.
- [16] D. W. MARQUARDT, *An Algorithm for Least-Squares Estimation of Nonlinear Parameters*, J. Soc. Ind. Appl. Math., 11 (1963), pp. 431–441.
- [17] H. MURAKAMI, *An Experiment of the Filter Diagonalization Method for the Banded Generalized Symmetric-Definite Eigenproblem*, Tech. Report 59(2007-HPC-110), Tokyo Metropolitan University, 2007.
- [18] H. MURAKAMI, *A Filter Diagonalization Method by the Linear Combination of Resolvents*, IPSJ Trans. ACS, 49 (2008), pp. 66–87.
- [19] H. MURAKAMI, *The Filter Diagonalization Method for the Unsymmetric Matrix Eigenproblem*, Tech. Report 43(2008-HPC-115), Tokyo Metropolitan University, 2008.
- [20] H. MURAKAMI, *Experiments of Filter Diagonalization Method for Real Symmetric Definite Generalized Eigenproblems by the use of Elliptic Filters*, Tech. Report 2010-HPC-125, Tokyo Metropolitan University, jun 2010.
- [21] H. MURAKAMI, *Optimization of Bandpass Filters for Eigensolver*, Tech. Report 2010-HPC-124, Tokyo Metropolitan University, 2010.
- [22] E. POLIZZI, *Density-matrix-based Algorithm for Solving Eigenvalue Problems*, Phys. Rev. B, 79 (2009), p. 115112.
- [23] Y. SAAD, R. LI, Y. XI, E. VECHARINSKY, AND C. YANG, *EigenValues Slicing Library*. <http://www-users.cs.umn.edu/~saad/software/EVSL/>. Accessed: 2016-11-05.
- [24] T. SAKURAI AND H. SUGIURA, *A Projection Method for Generalized Eigenvalue Problems using Numerical Integration*, J. Comput. Appl. Math., 159 (2003), pp. 119–128.
- [25] P. T. P. TANG AND E. POLIZZI, *FEAST As A Subspace Iteration Eigensolver Accelerated by Approximate Spectral Projection*, SIAM. J. Matrix Anal. & Appl., 35 (2014), pp. 354–390.
- [26] Y. XI AND Y. SAAD, *Computing Partial Spectra with Least-Squares Rational Filters*, SIAM J. Sci. Comput., 38 (2016), pp. A3020–A3045.